IRCS ECHELLE SPECTROGRAPH AND DATA HANDLING

Tae-Soo Pyo

Subaru Telescope
National Astronomical Observatory

May 2003

Contents

List of Figures

List of Tables

1   Introduction

In this document, we describe basics of echelle spectroscopy and handling of echelle data obtained with IRCS. Echelle spectroscopy is a powerful method to provide wide coverage of wavelengths yet to achieve high spectral resolution.

The echelle section of IRCS covers the entire J, H, or K band with only one or two grating configurations while achieving the velocity resolutions of $15 - 60$ km s^{-1}. Multiple transitions of [Fe ii] in the H band or of H_2 in the K band can be observed simultaneously, allowing us to investigate kinematics and physical properties such as line excitation, density, temperature, extinction, etc.

Data reduction of echelle spectra is complicated. In addition to the difficulties in handling one dimensional spectroscopic data in general, we must take into account the effects like the one that each slit image has a curvature along its length. Cross-dispersed echelle spectra taken with a cross-disperser have curvatures along the direction of the wavelength as well.

2   MERITS OF CROSS-DISPERSED ECHELLE SPECTROGRAPHS

A useful figure of merit for a grating spectrograph is its throughput, which is the spectral resolving power multiplied by its entrance slit width (Vogt, 1987). It is given by

$$R\phi = \frac{Wm\lambda}{\sigma D} = \frac{d_{col}\cos\gamma(\sin\alpha + \sin\beta)}{D \cdot \cos\alpha},$$

(1)

where R is the resolving power, ϕ is the entrance slit width projected on the sky (radian), W is the projected length of the collimated beam on the grating, λ is the wavelength of order number m, σ is the groove spacing of the grating, D is the diameter of the telescope primary, d_{col} is the collimated beam diameter, α and β are the angles of incidence and diffraction, respectively, and γ is the out-of-plane angle (Figure 1 and 2). For the Littrow case ($\alpha = \beta = \theta_B, \gamma = 0$)

$$R\phi = \frac{2d_{col}\tan\theta_B}{D},$$

(2)

where θ_B is the blaze angle of the grating.

In order to achieve a larger throughput, a larger beam size and blaze angle are required. The beam size becomes the largest when the focal ratio of the collimator equals the effective focal ratio of the telescope, i.e., $F_{col} = F_{tel}$.

An echelle grating has a large blaze angle and has high throughput compared to the other conventional diffraction gratings of the same size. Moreover, it is possible to utilize two-dimensional detector array space more efficiently by using a cross-disperser for order

separation. The cross-disperser disperses the spectrum into the direction perpendicular to the echelle dispersion, allowing us to cover wide spectral ranges with a single exposure.

Telescope   Slit   Collimator

fcam

Camera

Grating

GN   β

α

Φ

D

dcol

W

ftel   fcol

ΘB

σ

D : diameter of the telescope
Φ: entrance slit width in radian
ftel : focal length of the telescope
dcol: diameter of the collimator
fcol: focal length of the collimator
W : length of the grating in the beam
ΘB: blaze angle of the grating
σ: groove spacing
α: incident angle
β: diffraction angle
fcam: focal length of the camera
GN : grating normal

Figure 1: Schematic drawing of a slit spectrograph with a reflection grating.
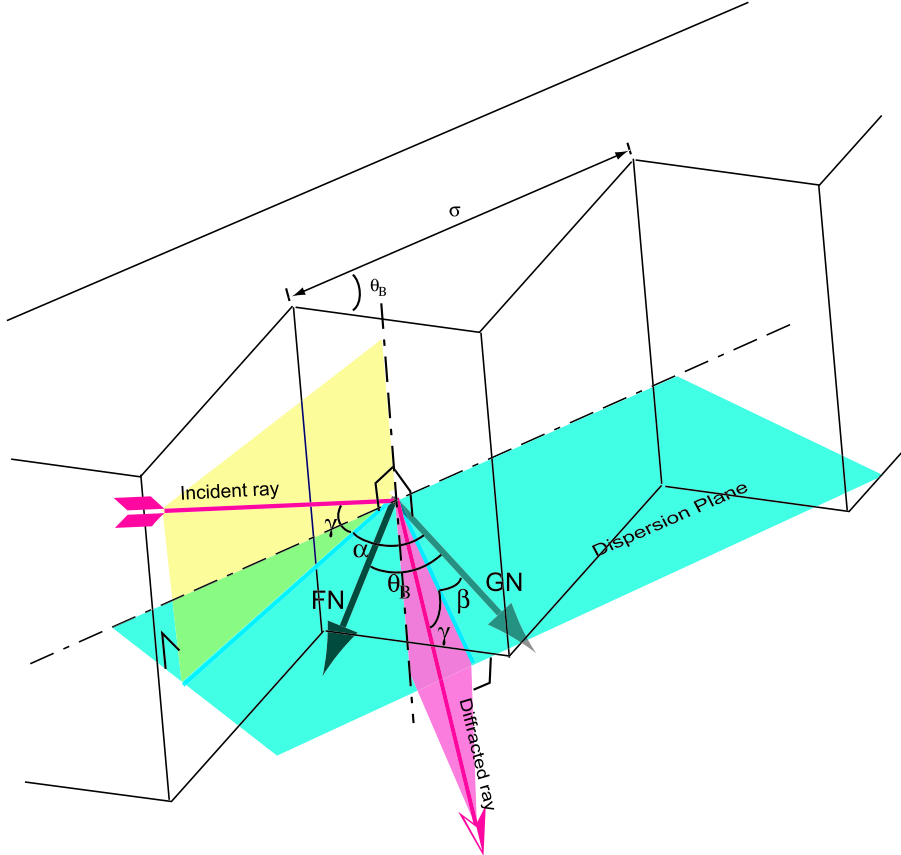
GN: Grating Normal, FN: Facet Normal
α: Incident Angle, β: Diffraction angle, γ: Out-of-Plane Angle
σ: Groove Spacing, θ_B: Blaze Angle

Figure 2: Schematic showing angles of incident angle α, diffraction angle β, and out-of-plane angle γ.

3 ECHELLE SPECTROGRAPH BASICS

This section describes how the spectral format, or *echellogram*, of the IRCS echelle section is disposed on a detector. We assume an echellogram imaged by a perfect optical system. Although a real optical system has aberrations, distortions, and miss-alignment of the optical axis (e.g. shift, rotation, tilt, etc.), a perfect optical system provides sufficiently meaningful reference and basis for us to understand the characteristics of the echellogram and to compare it with a real one.

3.1 The Equation of Echellogram

The echellogram of an echelle spectrograph with a perfect optics can be described by a simple combination of the dispersion equations of an echelle grating and a cross-disperser. The dispersion equation of the cross-disperser depends on its type. The equation of an echellogram, in addition, depends on the configuration of the two dispersing elements. In this dissertation, we will consider a grating equation for the case when a cross-disperser is placed after an echelle grating, i.e., the *post-disperser* configuration, in order to apply the results to IRCS which uses a low-dispersion grating as a cross-disperser.

We use the grating equation given by Schroeder (1987). The following equations represent the echellogram with x-axis being the direction of the echelle dispersion and y-axis being the direction of the cross-disperser dispersion.

$$x = f_{cam,e} \tan \left\{ \sin^{-1} \left(\frac{m_e \lambda}{\sigma_e \cos \gamma_e} - \sin \alpha_e \right) \right\} - x_o, \tag{3}$$

$$y = f_{cam,c} \tan \left\{ \sin^{-1} \left(\frac{m_c \lambda}{\sigma_c \cos \gamma_c} - \sin \alpha_c \right) \right\} - y_o, \tag{4}$$

where the subscript e and c mean echelle and cross-disperser, respectively, the position (x_o, y_o) is the detector center, γ is the out-of-plane angle, m is the order number, σ is the groove spacing, and α is the incident angle of a ray. Figure 2 shows the angles(α,β,γ) against a reflection grating. FThe parameters $f_{cam,e}$ and $f_{cam,c}$ are the effective focal lengths of the optics following the echelle and cross-disperser, respectively. For IRCS, $f_{cam,e}$ is equal to $f_{cam,c}$. They are not the same when there is optics that has pupil magnification between the echelle and cross-disperser gratings.
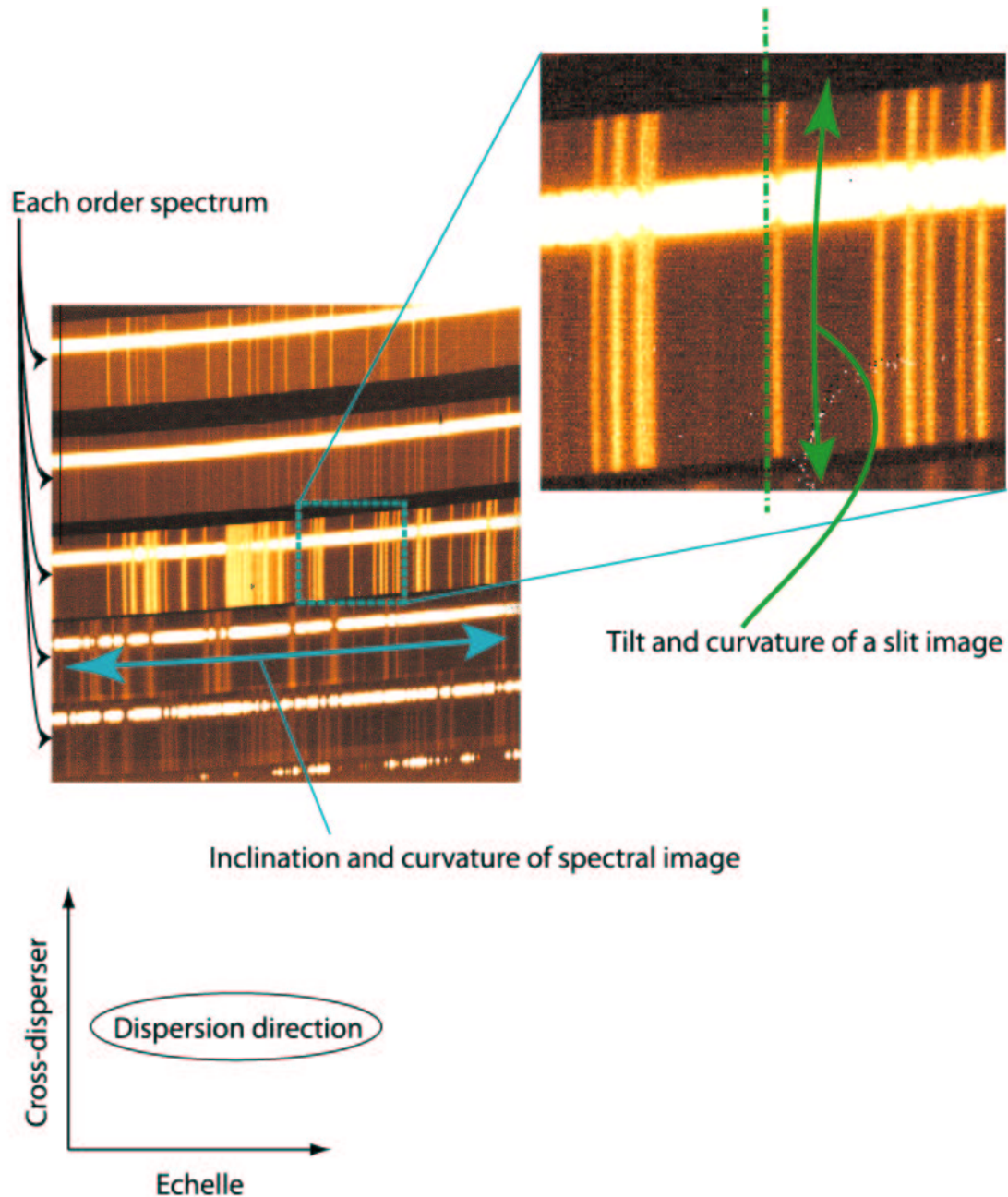
Figure 3: An echellogram of IRCS. The image is a L-band frame.

3.2 Inclination and Curvature of Spectral Images

Each order spectrum taken with a cross-dispersed echelle spectrograph has an inclination and curvature with respect to the dispersion direction of the echelle grating (Figure 3). The inclination is caused by the cross-disperser whose dispersion direction is perpendicular to that of the echelle grating in general. The inclination of the spectrum at a given wavelength is

$$\tan\psi = \frac{d\beta_c}{d\beta_e} = \frac{\sigma_e m_c}{\sigma_c m_e}\frac{\cos\gamma_e}{\cos\gamma_c}\frac{\cos\beta_e}{\cos\beta_c}. \tag{5}$$

From this equation, we know that the inclination increases with decreasing order number m_e, or increasing wavelength.

The curvature is caused mainly because the out-of-plane angle (γ_c) against the cross-disperser varies with wavelength in the beam which has already been dispersed by the echelle grating. Figure 4 shows the effect of out-of-plane angles on a spectrum. The out-of-plane angle against cross-disperser is given by

$$\gamma_c = (\beta_e - \beta_{x_o,e})/M_p + \gamma_{c0}, \tag{6}$$

where β_e is the diffraction angle of the echelle grating, $\beta_{x_o,e}$ is the diffraction angle toward the optical axis (center of the detector) against the echelle grating, γ_{c0} is the out-of-plane angle toward the optical axis (center of the detector) against the cross-disperser, and M_p is a pupil magnification between the echelle grating and cross-disperser. The dispersion angle β_c can be written as follows,

$$\beta_c(\lambda) = \beta_c(\lambda)|_{\gamma_c(\lambda)=\gamma_{c0}} + \Delta\beta_c(\gamma_c(\lambda)). \tag{7}$$

The dependence of β_c on γ_c is given as follows,

$$\frac{d\beta_c}{d\gamma_c} = \tan\gamma_c \lambda \frac{d\beta_c}{d\lambda}. \tag{8}$$

When γ_c changes from 0 to γ_χ ($\gamma_\chi \ll 1$), β_c changes roughly by the following amount,

$$\Delta\beta_c \approx \left(\frac{\gamma_\chi{}^2}{2}\right)\lambda A, \tag{9}$$

where A is the angular dispersion of the cross-disperser. Since γ_c is a function of $\beta_e - \beta_{x_o}$, the absolute value of γ_c takes its largest values at the both ends of the spectrum at each order. Thus, the spectrum is curved toward the longer wavelength side (+Y) as seen in Figure 4. When γ_{c0} is non-zero, the whole spectrum shifts to the longer wavelength (+Y) with its inclination changing. When γ_{c0} has a positive value, the spectrum will be steeper, because the absolute value of γ_c increases linearly with β_e. On the other hand, when γ_{c0} has a negative value, the absolute value of γ_c increases when $\beta_e < \beta_{X_o}$ and decreases when $\beta_e > \beta_{x_o}$. As a result, the inclination becomes gentler and eventually reverses with decreasing γ_{c0}.
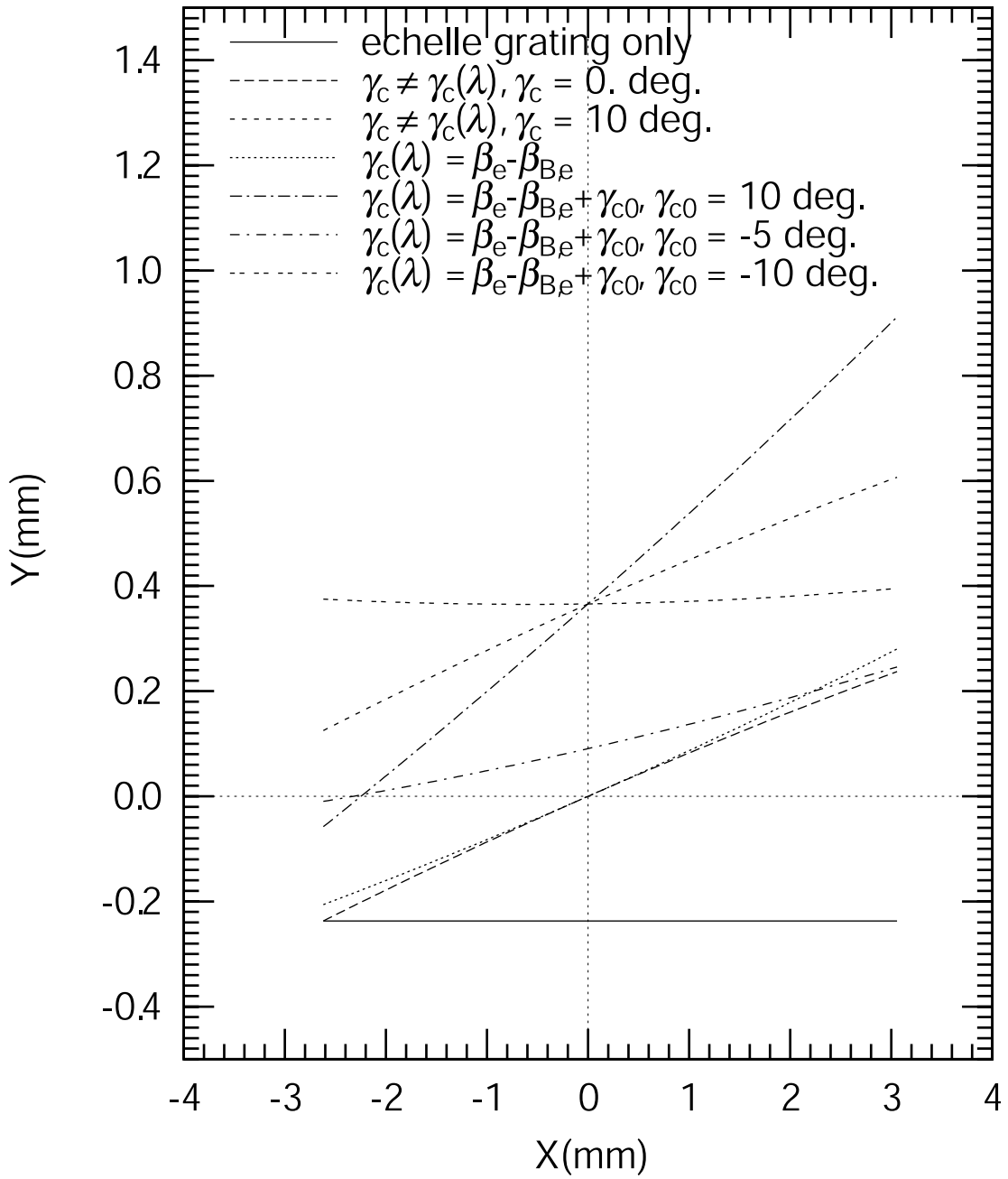
Figure 4: Variation of inclinations and curvatures with the out-of-plane angle of a cross-disperser. The diffraction angle increases with increasing X-coordinate. This graph is calculated with an echelle grating which has the groove number of 24.35 lines/mm and blaze angle of 70° (R2.75) and a cross-disperser which has the groove number of 150 lines/mm and blaze angle of 8°.63. We assumed $\beta_{B,e} = \beta_{x_o,e}$.

3.3 Separation between the Spectra of Two Adjacent Orders

When we use a reflection grating for the cross-disperser, the separation between the spectra of two adjacent orders is

$$\Delta y \;\; \approx \;\; f_{cam}\Delta\lambda\left(\frac{d\beta_c}{d\lambda}\right) \tag{10}$$

$$= \;\; f_{cam}\frac{{\lambda_1}^2\left(\frac{m_{e,1}}{m_{e,1}\pm 1}\right)}{\sigma_e\cos\gamma_e(\sin\alpha_e+\sin\beta_e)}\frac{m_c}{\sigma_c\cos\gamma_c\cos\beta_c}, \tag{11}$$

where $m_{e,1}\lambda_1 = (m_{e,1}\pm 1)\lambda_2$ and the subscript e and c denote the echelle and the cross-disperser, respectively. Definitions of the other parameters are the same as those in Eqs. 3 and 4. Since the variation of β_c on the detector can be ignored and $(m_{e,1}/m_{e,1}\pm 1)$ is nearly unity, the separation is simply proportional to the square of the wavelength and the order of the cross-disperser. We can control the separation of the spectrum by adjusting the order of the cross-disperser or exchanging cross-dispersers.

On the other hand, when a prism is used as a cross-disperser, the separation Δy is

$$\Delta y = f_{cam}\Delta\lambda\left(\frac{d\beta_c}{d\lambda}\right) \approx f_{cam}\frac{\lambda_B}{m}\left(\frac{t}{a}\frac{dn}{d\lambda}\right), \tag{12}$$

where $d\beta_c/d\lambda$ is the angular dispersion of the prism, t is the base length of the prism, a is the beam width, and n is the refraction index of the prism. Prisms have high and nearly constant efficiency which is principally related to the transmittance of the material. This allows us to use the detector area efficiently because the separation between the spectra increases more gradually than the case when we use a grating: the separation with a prism cross-disperser is proportional to λ and that with a grating is proportional to λ^2. Prisms are usually used for low spectral orders. In order to get sufficient separation, two prisms are used in sequence along the optical axis after an echelle grating or one prism is used before an echelle grating in order that the reflected and diffracted light by the echelle can be diffracted again.

In the UV and visual wavelengths, many echelle spectrographs use prisms for cross-dispersers: e.g. FEROS (Kaufer and Pasquini, 1998), FOCES (Pfeiffer et al., 1998), the echelle spectrograph of the MacDonald Observatory 2.7 m telescope (Tull et al., 1995), the Hamilton echelle (Vogt, 1987), etc. In the near infrared region a few echelle spectrograph use prisms for cross-dispersers: GRIS (Thompson et al., 1994), KSPEC (Hodapp et al., 1994), LEWIS (Imanishi et al., 1996), etc. Difficulty of using prisms in the near infrared region is because most optical materials have the minima in $dn/d\lambda$ in the near-infrared.

3.4 Shape of a Slit Image

The following equations represent the shape of a slit image,

$$x_s \;\; = \;\; f_{cam,e}\tan\left\{\sin^{-1}\left(\frac{m_e\lambda}{\sigma_e\cos(\gamma_e+\delta\gamma_e)}-\sin(\alpha_e+\delta\alpha)\right)\right\}-x, \tag{13}$$

16

$$y_s \;\; = \;\; f_{cam,c} \tan \left\{ \sin^{-1} \left(\frac{m_c \lambda}{\sigma_c \cos \gamma_c} - \sin(\alpha_c + \delta\gamma_e) \right) \right\} - y, \tag{14}$$

where (x_s, y_s) is the coordinates of the edge of the slit image relative to the center at (x, y), which are calculated by Eqs. 3 and 4. The parameters $\delta\alpha$ and $\delta\gamma_e$ are the angles corresponding to the half-width and half-length, respectively, of the slit against the echelle grating. The definitions of the other parameters are the same as those of Eqs. 3 and 4.

3.4.1   *Tilt and curvature of a slit image*

When a straight slit is located parallel to the ruling of a grating, an incident light ray passing through the slit toward the center of the grating has a finite out-of-plane angle (γ) defined by the distance between the position of the ray on the slit and the center. Due to the finite out-of-plane angle, the monochromatic slit image becomes tilted and curved (Figure 5). The tilt angle on the image is given as follows (Schroeder, 1987).

$$\tan \chi = \frac{d\beta}{d\gamma} = \tan \gamma \frac{\sin\alpha + \sin\beta}{\cos\beta}, \tag{15}$$

For the Littrow configuration ($\alpha = \beta = \theta_B$),

$$\tan \chi = 2 \tan \gamma \tan \theta_B, \tag{16}$$

at the blaze wavelength. Figure 6 shows that the tilt of a slit image is sensitive to the out-of-plane angle when the blaze angle of the grating is large.

Assuming that γ is small and integrating Eq. 15, we obtain

$$\Delta\beta \approx \left(\frac{\gamma^2}{2} \right) \lambda \frac{d\beta}{d\lambda}. \tag{17}$$

The slit image thus has a parabolic shape (Schroeder, 1987; Meaburn et al., 1984).

For a short slit, the slit image can be approximated by a tilted straight line. Figure 7 shows the variation of the tilt angle with the diffraction angle for an R2.0 echelle grating. It shows that the tilt angle becomes steeper with the diffraction angle when γ_e increases.

The tilted slit images complicate the reduction of a spectrum. It can be corrected by rotating the entrance slit by the angle χ. In this case, however, the spectral resolution is reduced because the entrance slit width along the direction of echelle dispersion increases by $w/\cos\chi$. In order not to reduce the spectral resolution, it is necessary to narrow the slit width by a factor of $\cos\chi$. This in turn reduces the flux by $\cos\chi$ and consequently the resolution-slit width product, i.e., the throughput, decreases by a factor of $\cos\chi$ (Schroeder & Hilliard, 1980).
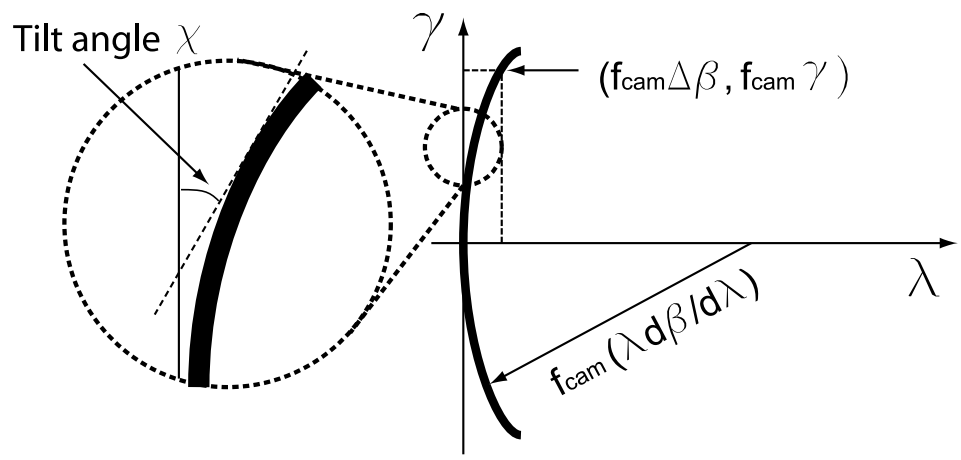
Figure 5: Tilt and curvature of a slit image.
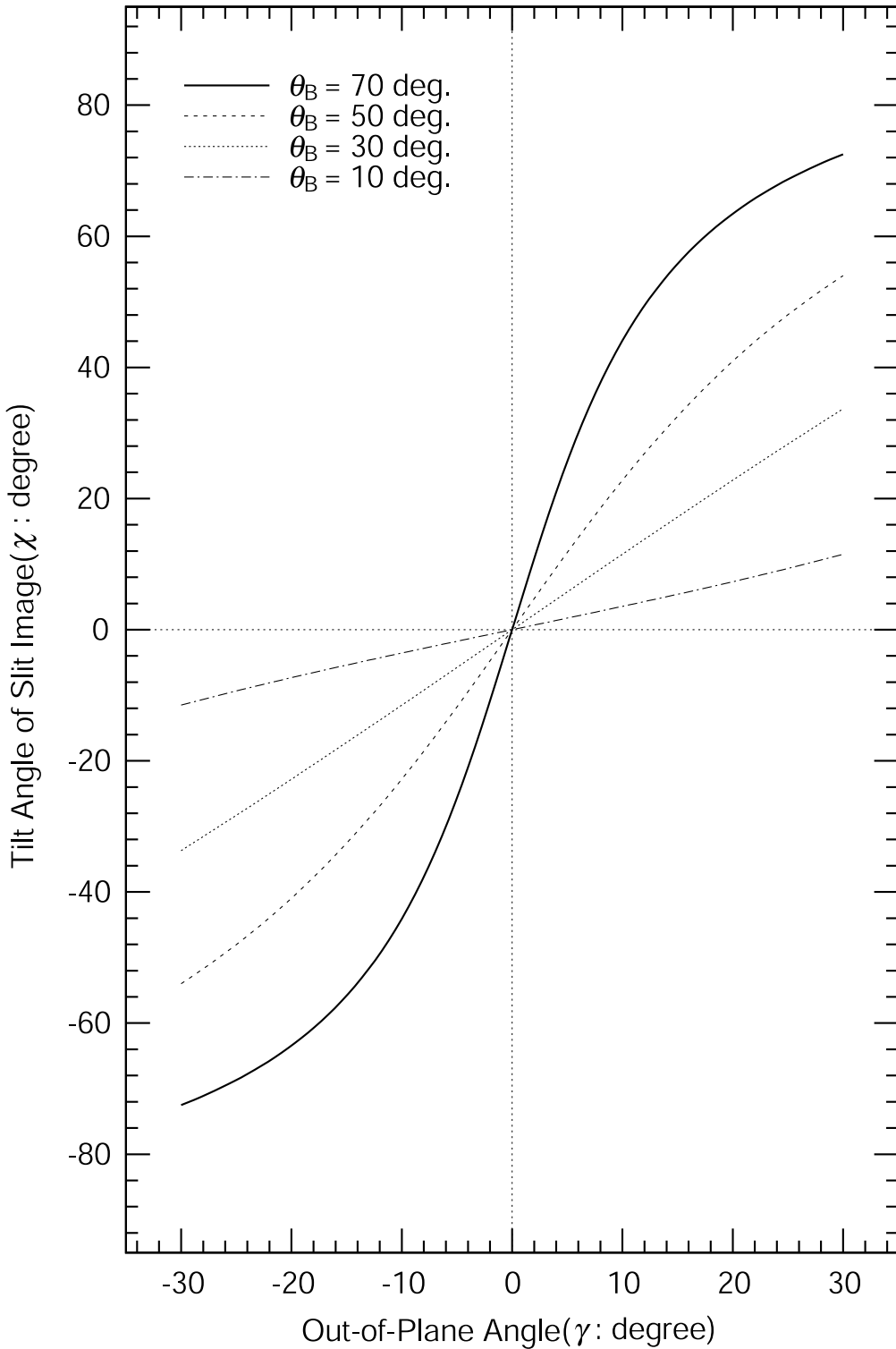
Figure 6: Variation of the tilt angle of a slit image with the out-of-plane angle (γ) and blaze angle (θ_B). The solid, dashed, dotted, and dash-dotted lines indicate the blaze angles of 70°, 50°, 30°, and 10°, respectively.
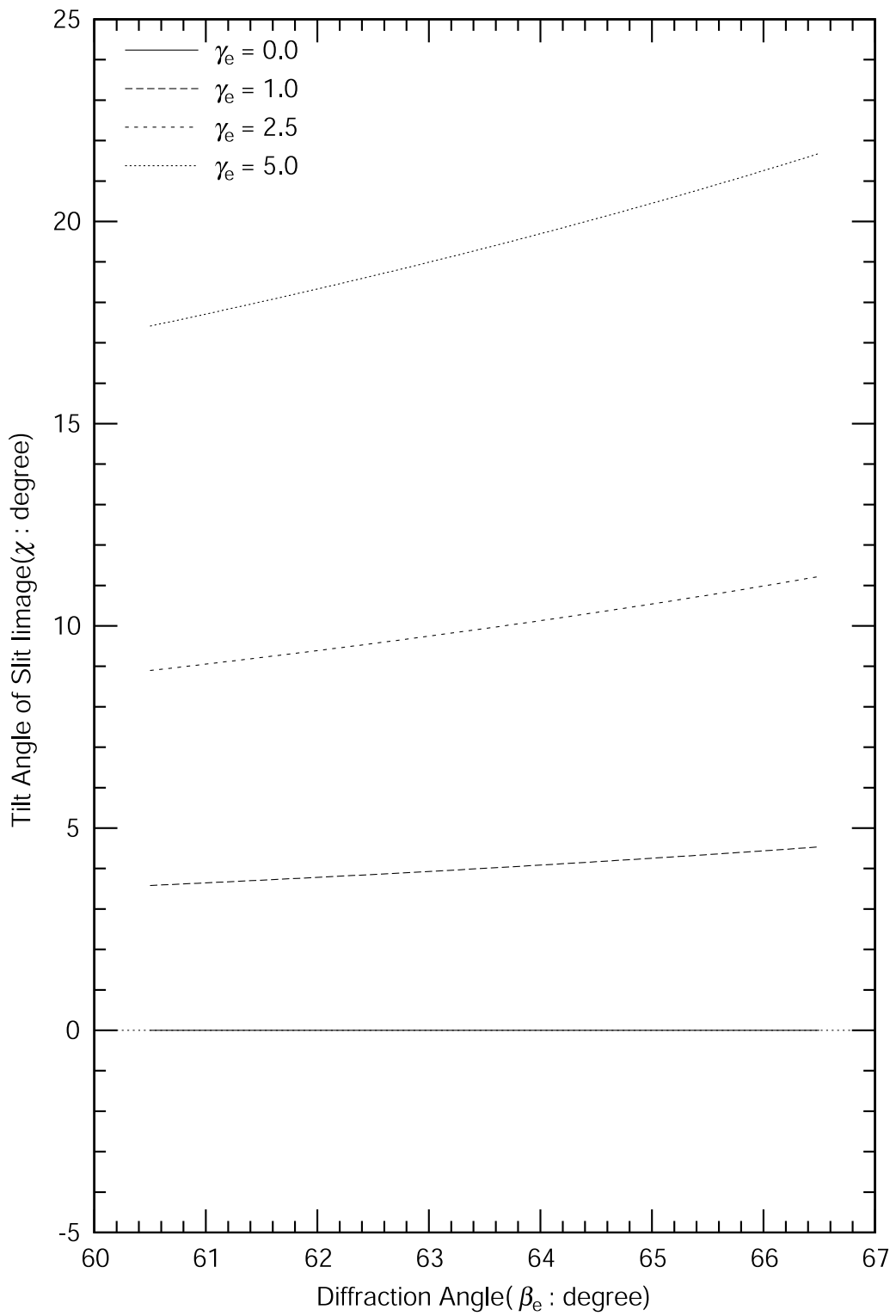
Figure 7: Variation of the tilt angle of slit images with diffraction angle for an R2.0 (blaze angle = $63^\circ\!.5$) echelle grating. The solid, long-dashed, short-dashed, and dotted lines indicate the out-of-plane angle γ_e of $0^\circ\!.0$, $1^\circ\!.0$, $2^\circ\!.5$, and $5^\circ\!.0$, respectively

3.4.2 *Width and length of a slit images: grating magnification*

The relation between the silt width and its image width is described as follows,

$$\frac{w'}{w} = \left(\frac{f_{cam,e}}{f_{col,e}}\right)\left(\frac{\cos\alpha_e}{\cos\beta_e}\right), \tag{18}$$

The $\cos\alpha/\cos\beta$ is called "anamorphic magnification" (Chaffee & Schroeder, 1976) or "grating magnification" (Wheeler, 1973). The width of a slit image increases with increasing grating magnification. Since the diffraction angle increases with wavelength, the width of a slit image becomes wider with increasing wavelength.

The length of the slit image is adopted in the same way. Since the dispersion of the cross-disperser is along the direction of the slit, the grating magnification of cross-disperser is adopted. The length of the slit image can then be written as

$$l' = \frac{l\left(\frac{f_{cam}}{f_{col}}\right)\left(\frac{\cos\alpha}{\cos\beta}\right)}{\cos\chi}. \tag{19}$$

where we take into account the tilt of the slit. The slit length magnification affects the pixel scale along the direction of the slit length.

Variations of the slit area and shape cause intensity variation and continuum contamination. For a uniform intensity source, the intensity per pixel will be affected by the grating magnification. This effect can be corrected by taking spectra of spectrophotometric standard stars that have flat continuum and weak spectral lines observed with the same spectrograph configuration as target objects.

3.5 Blaze Function and the Groove Shadowing Effect

The diffraction function is defined as a product of the blaze function and the grating interference function.

$$I = I(\delta) \cdot IF(\delta'). \tag{20}$$

The blaze function $I(\delta)$ determines a diffraction envelope and is given by

$$I(\delta) = \left(\frac{\sin\delta}{\delta}\right)^2, \tag{21}$$

where δ is the phase difference between the center and edge of a single groove of effective width s. The value of δ is given as,

$$\delta = \frac{\pi}{\lambda}s[\sin(\alpha - \theta_B) + \sin(\beta - \theta_B)], \tag{22}$$

where α is the incident angle, β is the diffraction angle, and θ_B is the blaze angle of the grating. The grating interference function is given by

$$IF = \left(\frac{\sin N\delta'}{N\sin\delta'}\right)^2, \tag{23}$$

where δ' is the phase difference between the centers of adjacent grooves and N is the number of grooves lighted up by incident beam on the grating. The value of δ' is given as follows,

$$\delta' = \frac{\pi}{\lambda}\sigma[\sin\alpha + \sin\beta], \tag{24}$$

where σ is the groove spacing.

For calculating the integrated intensity of spectral images, we use the peak intensity and effective image width of interference maxima. The peak values of the interference maxima are N^2. The effective image width of the mth order interference maximum, $\Delta\beta_m$, can be considered as a half of the separation of the first minima. The value of $\Delta\beta_m$ is,

$$\Delta\beta_m = \frac{\lambda}{N\sigma\cos\beta_m}, \tag{25}$$

where β_m is the diffraction angle of the mth order interference maximum. The integrated intensity of the mth order inerference maximum is given by

$$\begin{aligned} I_m &= I(\delta)\cdot N^2\cdot\Delta\beta_m \tag{26}\\ &= I(\delta)\cdot N^2\frac{\lambda}{N\sigma\cos\beta_m}. \tag{27} \end{aligned}$$

The form of the blaze function I(δ) is dependent on the relation between incident and diffract angles as seen in below.
(a) Case for $\alpha > \beta$
The effective groove width s varies with the incident angle (Figure 8) and can be written as

$$s = \frac{\sigma\cos\alpha}{\cos\theta}, \tag{28}$$

where θ is $\alpha - \theta_B$. The blaze function will thus be

$$I(\delta) = sinc^2\left(\frac{\pi}{\lambda}\frac{\sigma\cos\alpha}{\cos\theta}[sin(\alpha - \theta_B) + sin(\beta - \theta_B)]\right). \tag{29}$$

(b) Case for $\alpha < \beta$
In this case, the diffracted beam is vignetted by neighboring grooves (Figure 8) and only the fraction $\cos\beta/\cos\alpha$ contributes to the image (Bottema, 1981). The effective groove width s is determined by the diffracted beam and can be written in the form similar to Eq. 28.

$$s = \frac{\sigma\cos\beta}{\cos\theta}. \tag{30}$$

The blaze function will be

$$I(\delta) = \frac{\cos\beta}{\cos\alpha}sinc^2\left(\frac{\pi}{\lambda}\frac{\sigma\cos\beta}{\cos\theta}[sin(\alpha - \theta_B) + sin(\beta - \theta_B)]\right). \tag{31}$$

22

The peak values of interference maxima are also smaller than those for the case $\alpha > \beta$. As a result, the integrated intensity will be

$$I_m = \left(\frac{\cos\beta}{\cos\alpha}\right)^2 \cdot I(\delta)' \cdot N^2 \Delta\beta_m, \tag{32}$$

where $I(\delta)' = I(\delta) \cdot (\cos\alpha / \cos\beta)$.

The effective blaze function (EBF) can be written as follows,

$$\text{EBF} = \begin{cases} sinc^2\left(\frac{\pi}{\lambda}\frac{\sigma\cos\alpha}{\cos\theta}[\sin(\alpha - \theta_B) + \sin(\beta - \theta_B)]\right) & \text{if } \alpha \geq \beta \\ \left(\frac{\cos\beta}{\cos\alpha}\right)^2 sinc^2\left(\frac{\pi}{\lambda}\frac{\sigma\cos\beta}{\cos\theta}[\sin(\alpha - \theta_B) + \sin(\beta - \theta_B)]\right) & \text{if } \alpha < \beta \end{cases} \tag{33}$$

where the peak value of the interference maxima are normalized to N^2.

Figure 9 shows the EBF when $\theta = 0$ and 4 degrees. When $\alpha < \beta$, the amplitude of the EBF is a factor of $(\cos\beta / \cos\alpha)^2$ smaller than that of the EBF for $\alpha \geq \beta$, and the effective width of a single groove gets narrower with increasing β. As a result, the main envelope of the EBF for $\alpha < \beta$ gets broader for lower amplitudes and the side-lobes are negligible.

The blaze function is affected by polarization. The polarization effect is related to the ratio of wavelength to groove spacing, λ/σ, and the blaze function. The scalar theory can be used as a good approximation when λ/σ is less than 0.2 (Loewen et al., 1977). For the Littrow case, the ratio can be re-written as follows

$$\frac{\lambda_B}{\sigma} = \frac{2\sin\theta_B}{m}. \tag{34}$$

Thus the polarization effect is negligible for high orders. For examples, the ratio is less than 0.2 when $m > 10$ for an R2.00 echelle ($\theta_B = 63.435$) and an R2.75 echelle ($\theta_B = 70.0$).

GN

GN

β_1

α

θ_B

FN

S_1

α

β_2

S_2

σ

θ_B

S_1 : effective groove width when $\beta < \alpha$
S_2 : effective groove width when $\beta > \alpha$
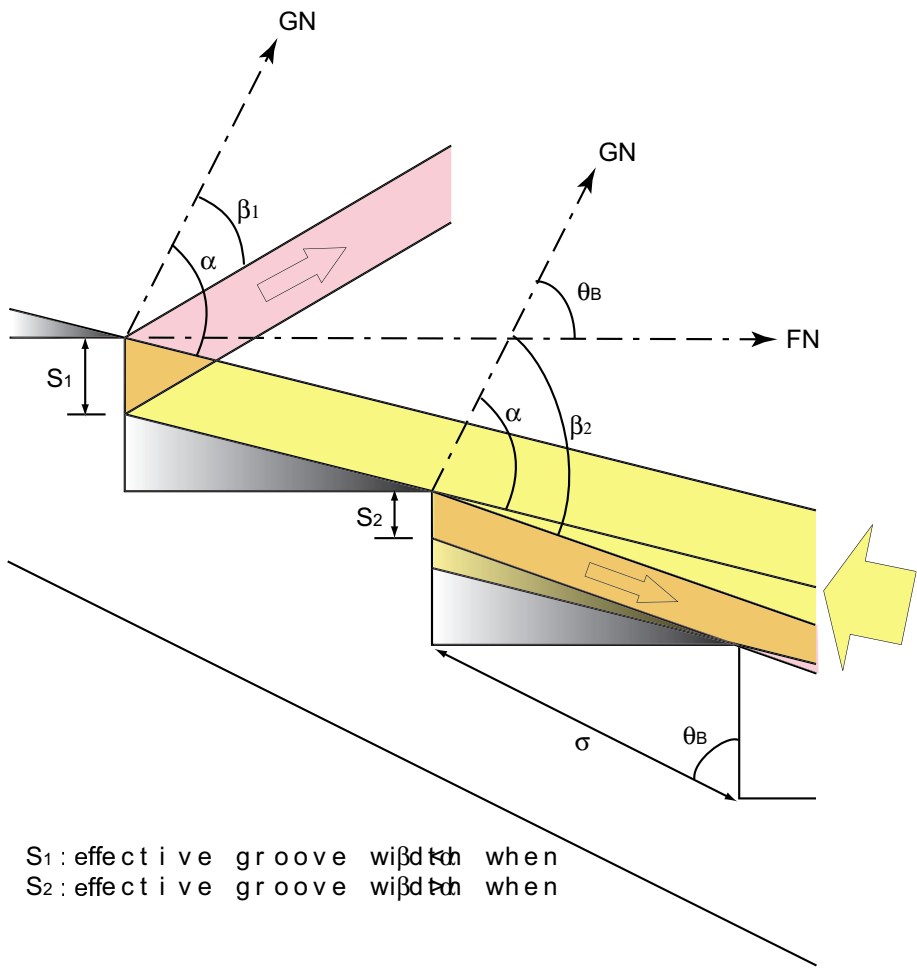
Figure 8: Effective groove widths with incident and diffraction angles.
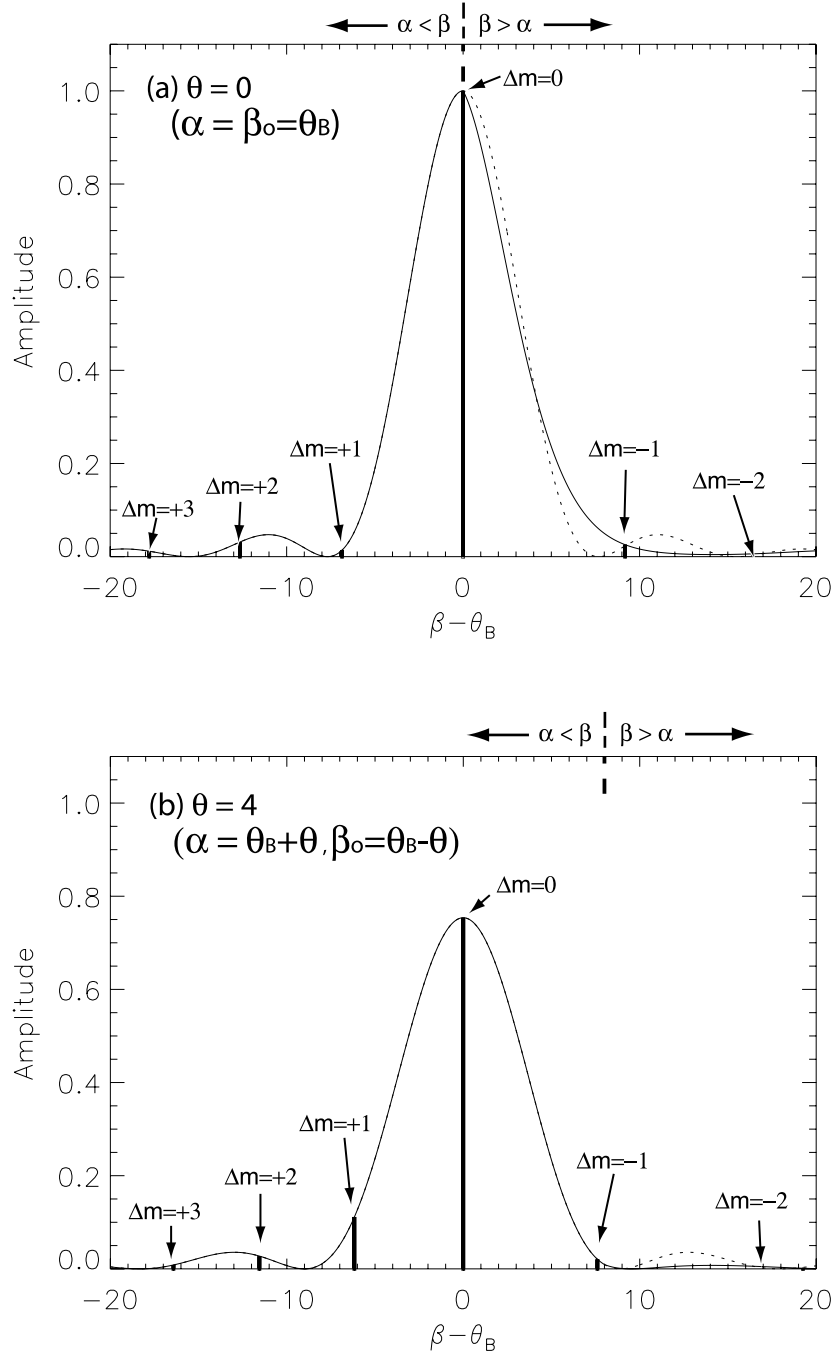
Figure 9: The effective blaze functions and locations of the interference mazima when (a) $\theta = 0$ degrees and (b) $\theta = 4$ degrees for m = 30 with R2.00 echelle grating . The thin solid lines indicate effective blaze function considered the shadowing effect, which is represented by Eq. 33. The dotted lines indicate blaze functions without shadowing effect. The thick solid vertical lines indicate the interference pattern.The dashed lines indicate the angles when $\alpha = \beta$.

3.6   Blaze Peak Efficiency

The total intensity in a diffracted beam at the blaze wavelength is given by the sum of integrated intensity of all possible orders within $\theta_B - 90° < \beta < 90°$.

$$I_t = N^2 I(0)\Delta\beta_0 \left\{ 1 + \sum_{\delta\neq0}^{\alpha>\beta_m} \frac{I(\delta)}{I(0)} \frac{\Delta\beta_m}{\Delta\beta_0} + \sum_{\delta\neq0}^{\alpha<\beta_m} \left(\frac{\cos\beta_m}{\cos\alpha}\right)^2 \frac{I(\delta)'}{I(0)} \frac{\Delta\beta_m}{\Delta\beta_0} \right\}. \qquad (35)$$

where $I(0)$ is the peak intensity at the blaze direction β_0. The blaze peak efficiency is defined as follows by Schroeder (1981),

$$E = \frac{N^2 I(0)\Delta\beta_0}{I_t} \qquad (36)$$

$$= \left\{ 1 + \sum_{\delta\neq0}^{\alpha>\beta_m} I(\delta)\frac{\cos\beta_0}{\cos\beta_m} + \sum_{\delta\neq0}^{\alpha<\beta_m} \left(\frac{\cos\beta_0}{\cos\beta_m}\right)^2 I(\delta)'\frac{\cos\beta_0}{\cos\beta_m} \right\}^{-1}, \qquad (37)$$

where I(0) = 1.

3.6.1   *Variation of the blaze peak efficiency with θ $(= \alpha - \theta_B)$ and γ*

We calculated the blaze peak efficiencies for R2.00 and R2.75 echelles. Figures 10 and 11 show the variation of the blaze peak efficiency with θ $(= \alpha - \theta_B)$ for R2.00 and R2.75 echelles, respectively. The blaze peak efficiency decreases with $\cos\alpha/\cos\beta$ with increasing θ. These results confirm the results of Schroeder (1981) and prediction of Bottema (1981). The decrease of the blaze peak efficiency with θ is explained as follows. The effective width of a groove gets smaller with increasing θ, so that the blaze function gets broader. Thus the interference maxima for $\Delta m = \pm1$ are located inside the main diffraction envelope as shown in Figure 9. The integrated intensities for $\Delta m = \pm1$ and ±2 are shown in Figures 12 and 13 for $\theta = 0$, $2 - 6$. As seen in Figure 12 and 13, the integrated intensities for the $\Delta m = \pm1$ orders increase significantly with increasing θ. As a result, the blaze peak efficiency decreases with increasing θ (Figures 10 and 11).

Figures 14 and 15 show the variation of the blaze peak efficiency with γ. The efficiency varies only a few percent with γ.

In Figures 10 and 11, several dips exist on the curves with their location changing with the spectral order. In Figures 14 and 15, the blaze peak efficiencies vary with spectral orders. These are related to Wood's anomallies, which are discussed in the following subsection.
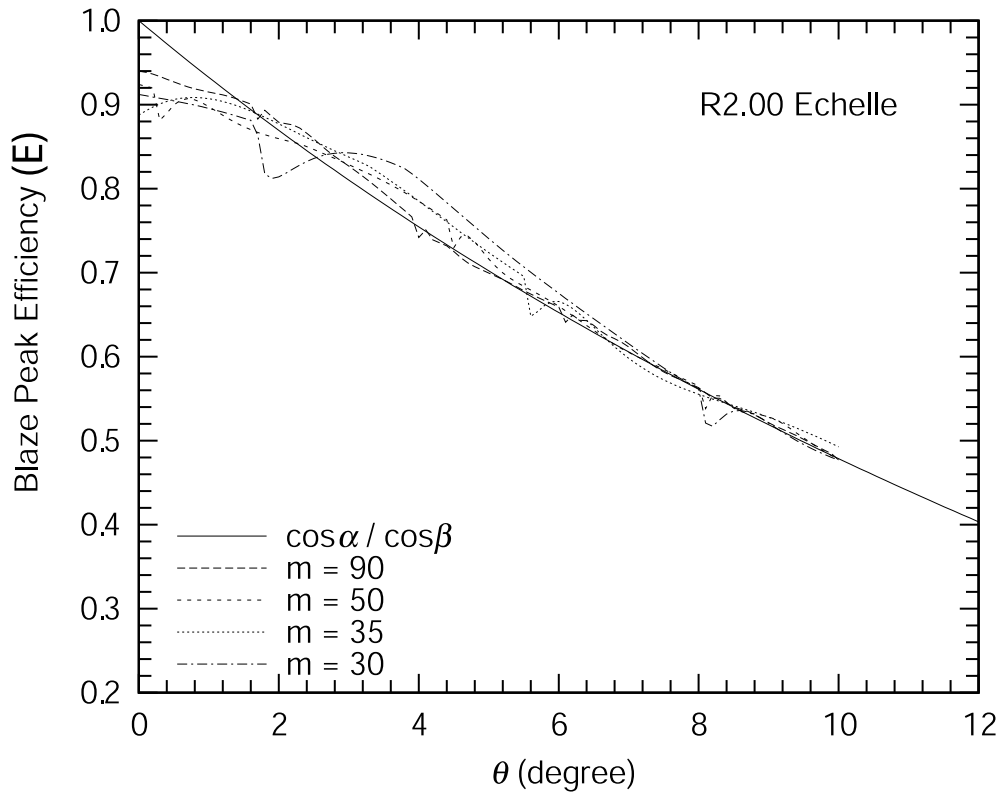
Figure 10: Variation of the blaze peak efficiency with θ ($= \alpha - \theta_B$) for an R2.00 echelle.
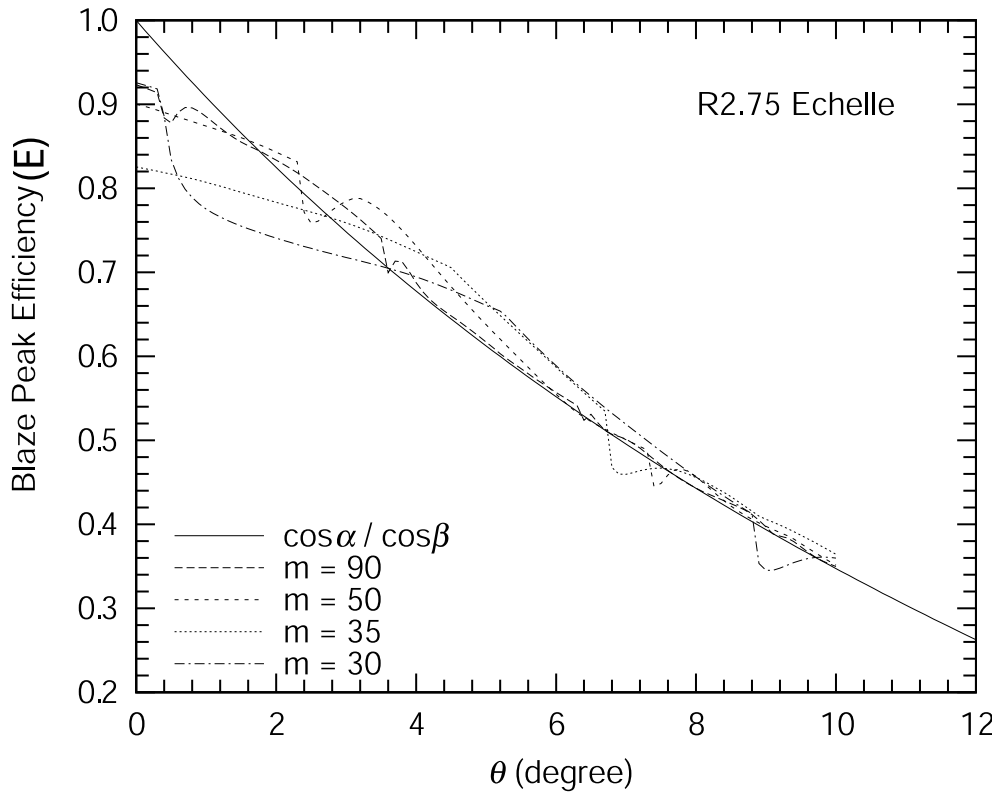
Figure 11: Variation of the blaze peak efficiency with θ $(= \alpha - \theta_B)$ for an R2.75 echelle. $\bar{m} = m$.
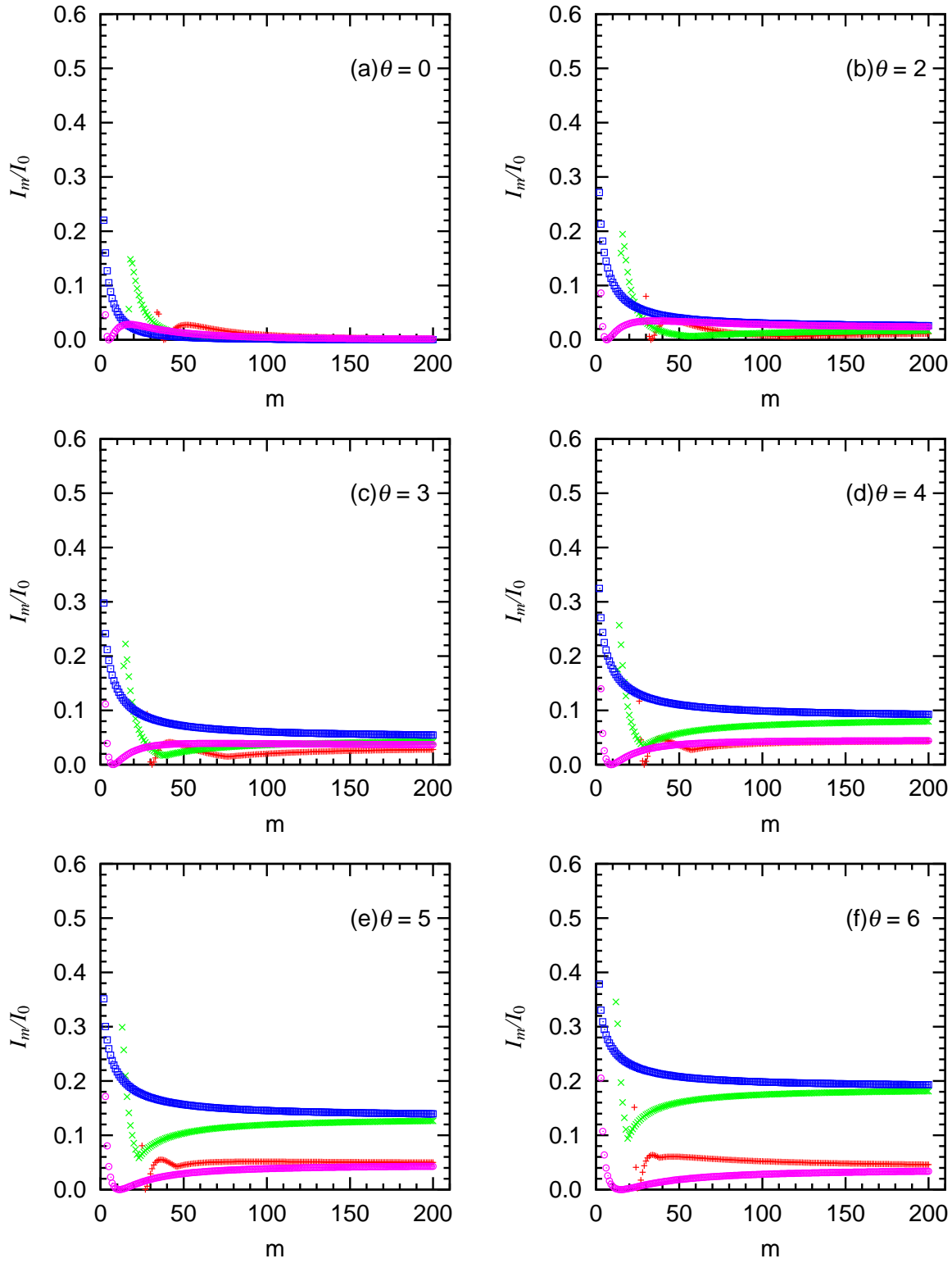
Figure 12: I_m/I_0 for the R2.00 echelle when $I_0 = 1$. I_m is the integrated intensity of the sub-order Δm: $N^2 I(\delta)\Delta\beta_m$. I_0 is the integrated intensity at the main peak($\Delta m = 0$): $N^2 I(0)\Delta\beta_0$. $+$ (red): $\Delta m = -2$, $\times$ (green): $\Delta m = -1$, $\boxdot$ (blue): $\Delta m = +1$, $\odot$ (pink): $\Delta m = +2$.
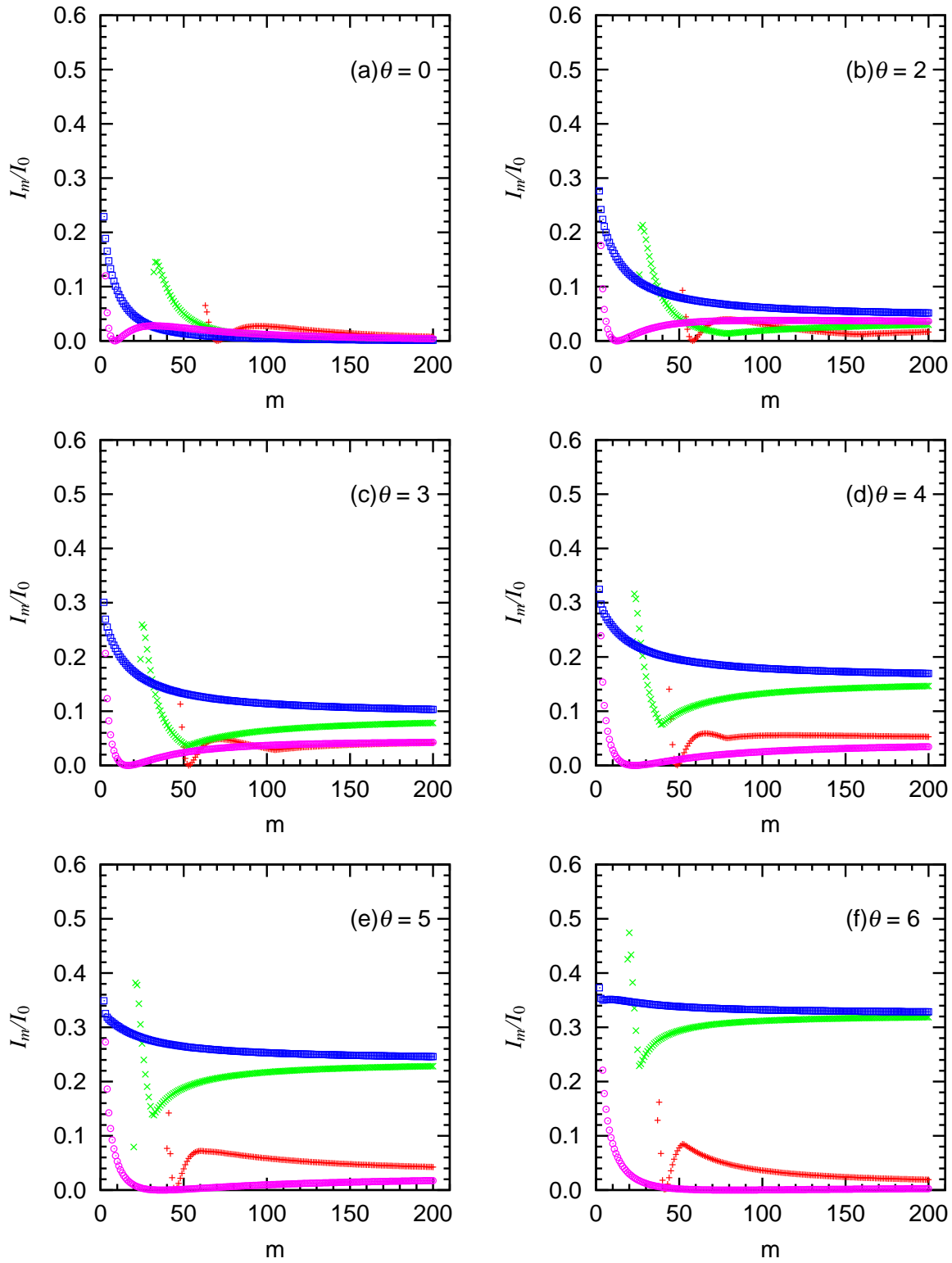
Figure 13: I_m/I_0 for the R2.75 echelle. The marks have the same meanings as for Figure 12.

30
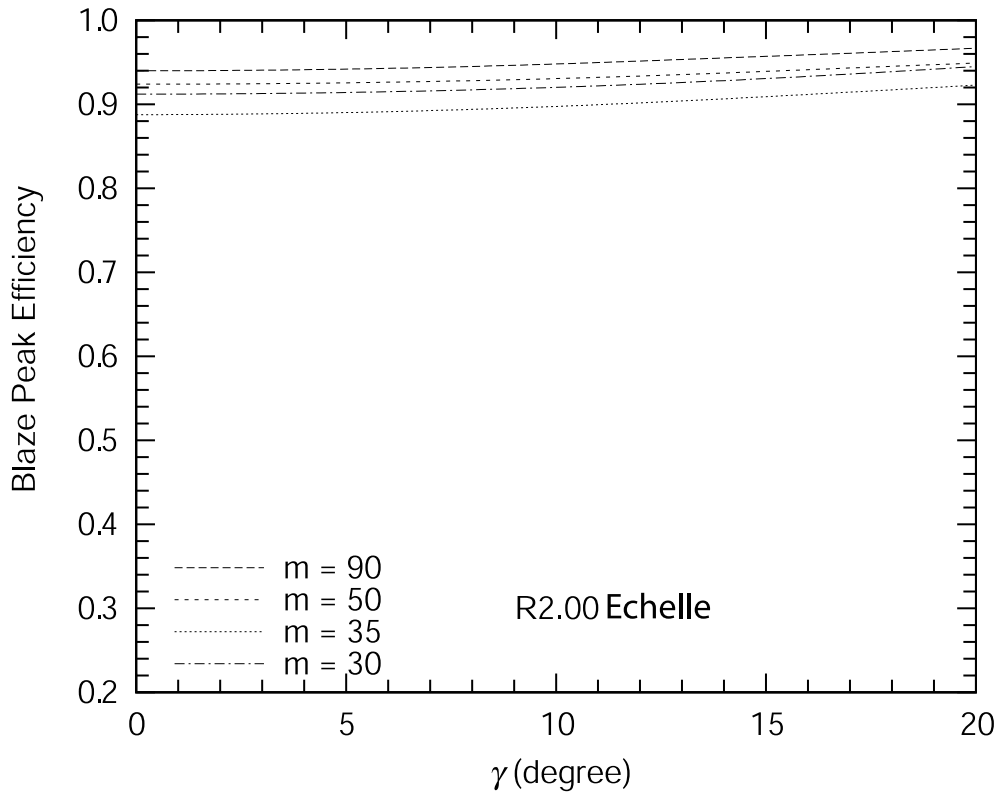
Figure 14: Variation of the blaze peak efficiency with out-of-plane angle γ for an R2.00 echelle.
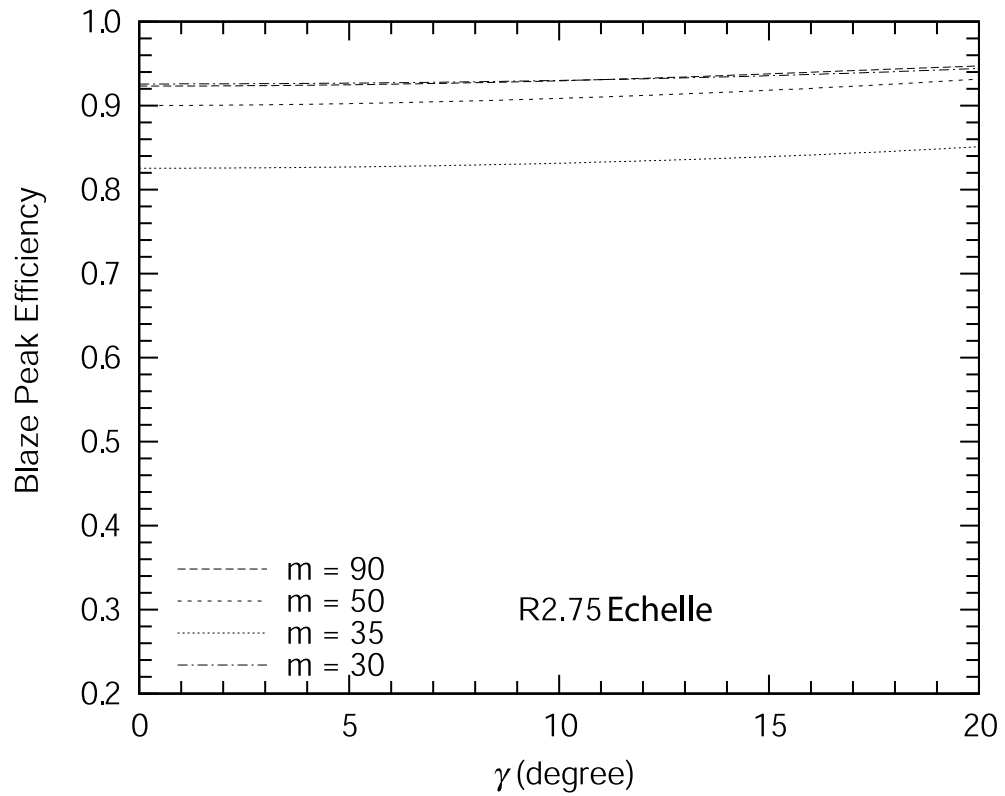
Figure 15: Variation of the blaze efficiency with out-of-plane angle γ for an R2.75 echelle.

3.6.2 *Variation of the blaze peak efficienty with spectral orders and Wood's anomaly*

The variation of efficiency with spectral order is shown in Figures 16 and 17, in which several dips are seen on the blaze peak efficiency curves. The dips get deeper and wider with decreasing spectral order.

These dips are related to Wood's anomallies discovered by Wood in 1902 as a phenomenon that the intensity distribution of the diffracted light varies abruptly. Description about these anomallies is seen in Kitchin (1995):

> ".... These are sudden brightenings of the spectrum with a sharp onset and a slightly less sharp decline to longer wavelengths. The anomallies arise from that energy that would go into spectral orders behind the grating, if these were possible, being redistributed back into the actually visible orders. ...."

The first sentence in the above quotation exactly corresponds to the shape of the dips. In order to confirm the fact that the dips are caused by Wood's anomallies, locations of the anomallies are calculated. The spectral orders at which the anomallies occur can be calculated by the following equations,

$$m_{+} = \frac{\sigma \cos \gamma}{\lambda_B}(\sin \alpha + 1), \tag{38}$$

$$m_{-} = \frac{\sigma \cos \gamma}{\lambda_B}(\sin \alpha + \sin(\theta_B - 90)), \tag{39}$$

where m_+ is the order number at $\beta = 90°$, m_- is the order number at $\beta = \theta_B - 90°$, λ_B is the blaze wavelength at m, and γ is the out-of-plane angle. Because $\lambda_B = (\sigma \cos \gamma/m) \cdot 2 \sin \theta_B \cos \theta$,

$$m - m_{+} = m\left(1 - \frac{\sin \alpha + 1}{2 \sin \theta_B \cos \theta}\right), \tag{40}$$

$$m - m_{-} = m\left(1 - \frac{\sin \alpha + \sin(\theta_B - 90)}{2 \sin \theta_B \cos \theta}\right). \tag{41}$$

The locations are shown in Figures 18 and 19 with arrows. By comparison, it is confirmed that the dips occur at the expected positions where Wood's anomallies occur. The anomallies are strong for lower Δm because the interference maxima for lower Δm exist in the higher intensity region of the diffraction envelope. The biggest dips and brightenings at the 18th order for an R2.00 echelle and at the 30th order for an R2.75 echelle are related to the anomallies that the interference maximum for the spectral order $\Delta m = -1$ disappears beyond the dispersion limit ($\theta_B - 90° < \beta < 90°$) with decreasing $\bar{m}$ (see Figures 12 and 13) and the intensity is re-distributed into remnants of the interference maxima within the dispersion limit.

The locations of the anomallies are shifted toward lower orders with increasing θ as seen in Figures 16 and 17. The blaze peak efficiency in the dips is less than the value of $(\cos \alpha / \cos \beta)$.
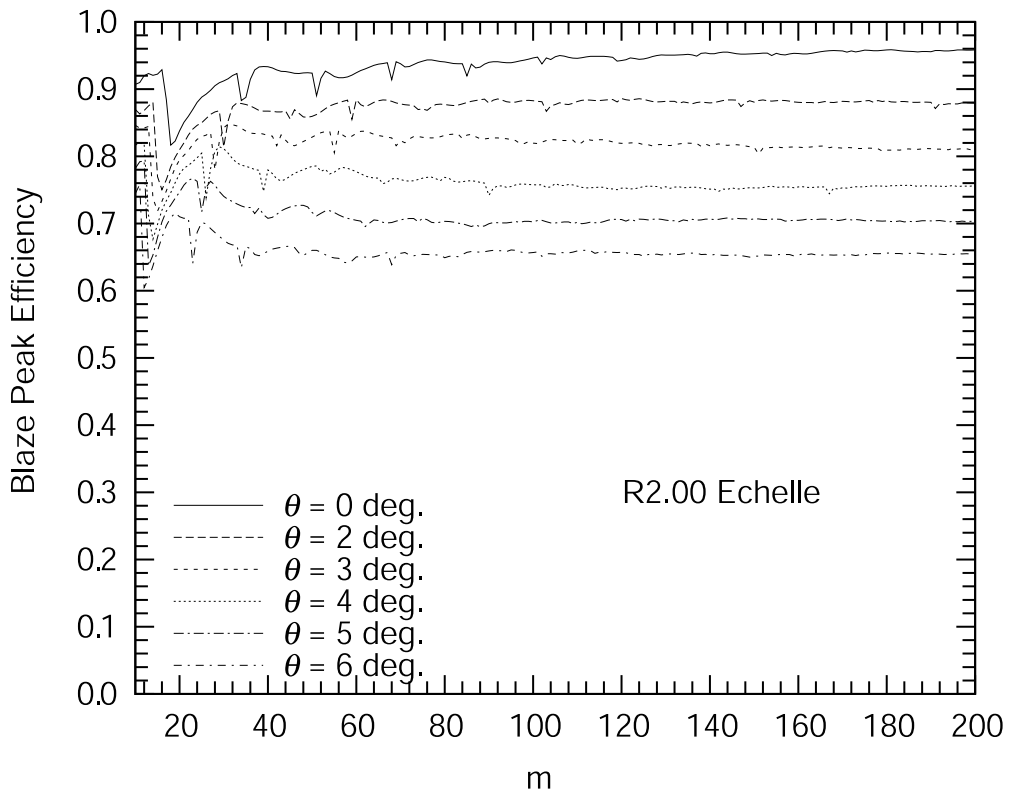
Figure 16: Variation of the blaze peak efficiency with order number for an R2.00 echelle.
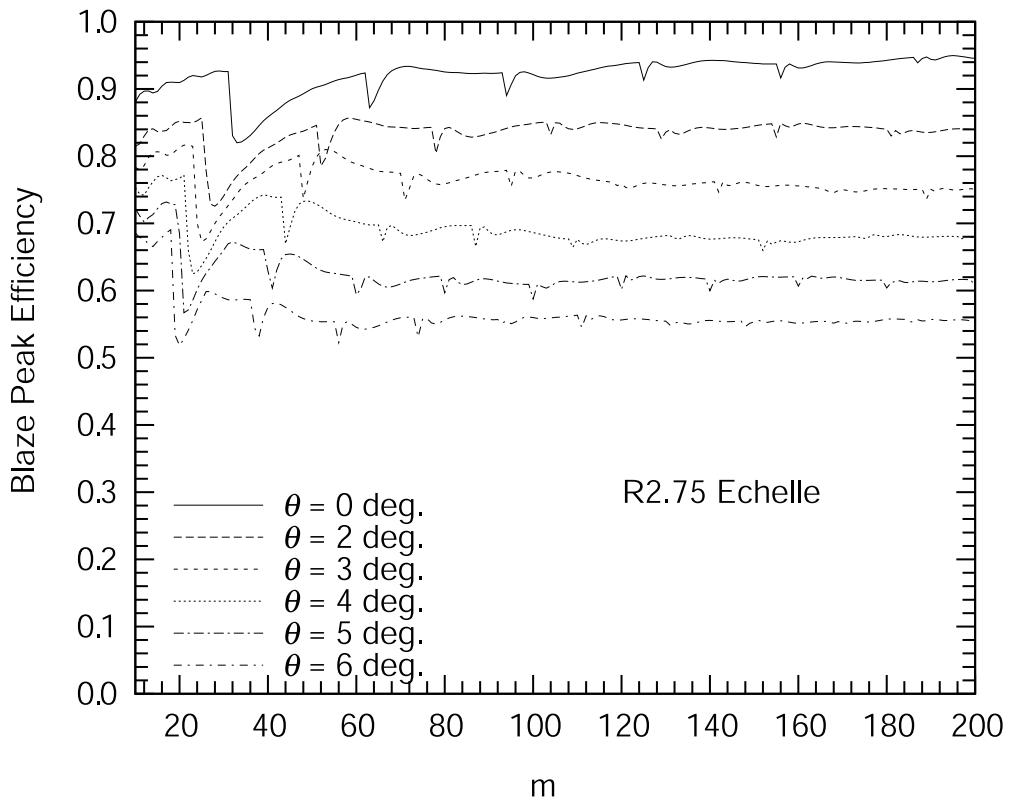
Figure 17: Variation of the blaze peak efficiency with order number for an R2.75 echelle.
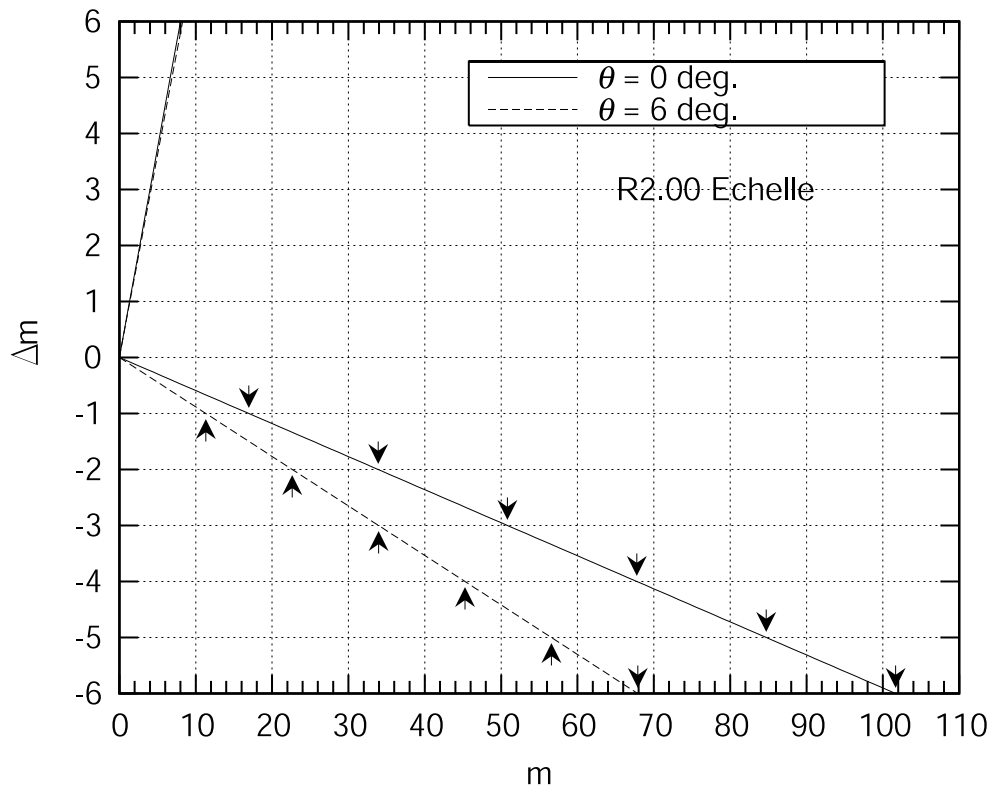
Figure 18: Locations of Wood's anomallies for an R2.00 echelle. Arrows indicate their positions.
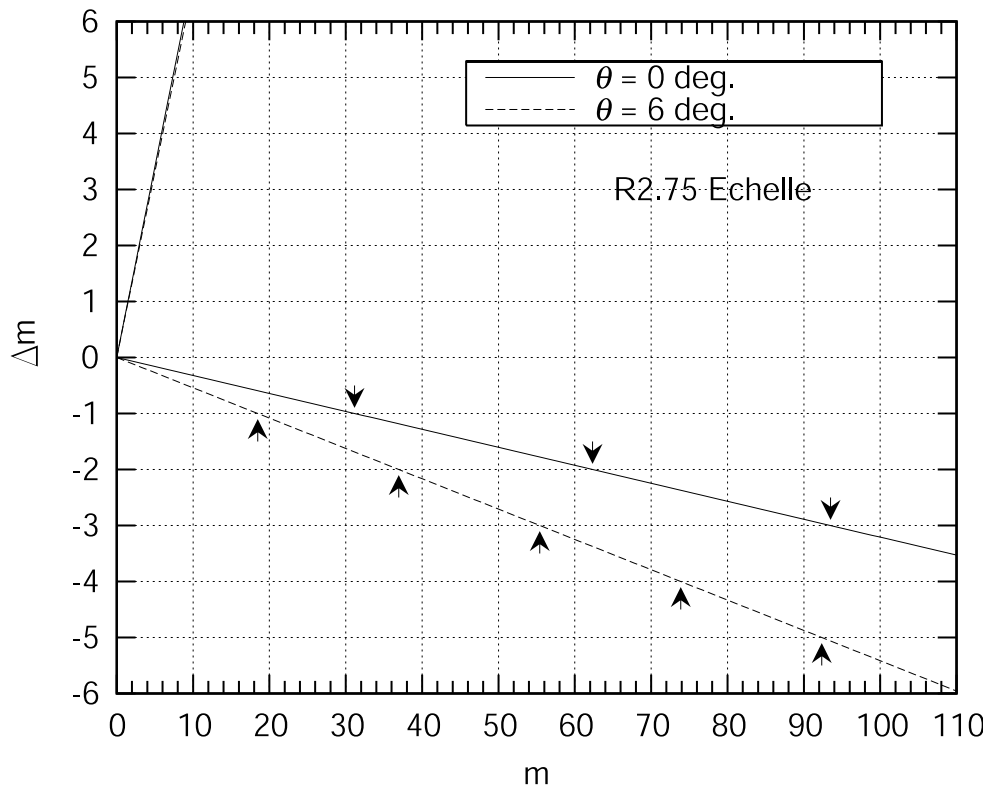
Figure 19: Locations of Wood's anomallies for an R2.75 echelle. Arrows indicate their positions.

4 IRCS ECHELLE SPECTROGRAPH

4.1 IRCS Overview

IRCS (Infrared Camera and Spectrograph) is a facility instrument of the Subaru Telescope, providing high-resolution imaging and spectroscopy with the adaptive optics (AO) and tip-tilt at $0.9 - 5.5$ μm.

IRCS consists of two sections (Figure 20). One is a near-infrared camera with two available pixel scales: 0.058 and 0.023 $''$/pix. The camera section also serves as an infrared slit-viewer for echelle spectroscopy. The infrared slit-viewer is very useful to locate slit positions. The camera section also provides low spectral resolution grism spectroscopy in the near infrared.

The other is a cross-dispersed echelle spectrograph that provides high velocity resolutions ($15-60$ km s^{-1}). The echelle section has a pixel scale of 0.060 $''$/pix along the slit length, allowing us to study detailed velocity structure of $\sim$10 AU scale around YSOs in Taurus molecular cloud. The echelle part covers the entire J-, H-, or K-band with only one or two echelle configurations (Table 1). The slit length is variable from $3''\!.8$ to $10''\!.0$.

Each section is equipped with a Raytheon 1024×1024 InSb IR array with an Aladdin multiplexer.

Table 1: IRCS echelle configurations.

Band	Coverage (μm)	Spectral resolution ($0''\!.15$ slit)	Dispersion (Å/pixel)	Slit length (arcsec)	No. of exposures
$Iz(1)$	$0.92 - 1.01$	$\sim$20000		3.8	1
zJ	$1.03 - 1.18$	$19000 - 22600$	$0.25 - 0.28$	3.8	1
J	$1.18 - 1.38$	$19000 - 22600$	$0.28 - 0.33$	3.8	1
H	$1.49 - 1.83$	$18800 - 22900$	$0.36 - 0.44$	5.6	2
K	$1.90 - 2.49$	$18300 - 22300$	$0.46 - 0.62$	5.6	2
L	$2.80 - 4.20$	$17300 - 25100$	$0.67 - 1.06$	10.0	6
M	$4.41 - 5.34$	$16800 - 26300$	$1.16 - 1.30$	10.0	4

(a) The fore-optics and camera sections

ENTRANCE WINDOW
BEAMSPLITTER
TELESCOPE FOCUS
TO WAVE FRONT SENSOR
EXIT WINDOW
COMPENSATOR
OFFNER SECONDARY
OFFNER PRIMARY
FOLD MIRROR
FOLD MIRROR
FIELD LENS
FOLD MIRROR
COLLIMATOR LENSES
FILTER WHEELS
INTERNAL TRUSS
FLIP MIRROR
0.060"/PIXEL
0.022"/PIXEL
IR ARRAY
FOLD MIRROR
FLIP MIRROR
CAMERA OPTICAL TABLE
FOLD MIRROR
SUPPORT PLATE

(b) The spectrograph section

IR ARRAY
ECHELLE
FOLD MIRROR
FOUR-MIRROR ANASTIGMAT
FILTER WHEEL
SLIT WHEEL
COLLIMATOR
CROSS DISPERSOR
SUPPORT PLATE
SPECTROGRAPH OPTICAL TABLE

Figure 20: Layout of (a) the fore-optics and camera sections and (b) the spectrograph section (Tokunaga et al., 1998).

39

4.2   Optimized Grating Operation Angle

Most echelle spectrographs operate near the blaze angle (=groove angle) of the echelle grating, *near-Littrow or Quasi-Littrow Configuration*, to maximize diffraction efficiency and minimize anamorphic magnification. The incident angle α should be greater than the diffraction angle β to avoid efficiency loss due to the groove shadowing effect (Schroeder & Hilliard, 1980; Schroeder, 1987).

The IRCS echelle operates around $63°.5$ with $(\alpha-\beta)_{e0} = 8°$ to allow sufficient separation between the incident and diffracted beams in a reasonable distance while keeping the configuration as close as possible to the Littrow condition. The operating angle of the cross-disperser is about $31°$ with the incident angle of $24°$ at the blaze wavelength. These angles were determined somewhat arbitrarily considering the mechanical arrangement of optical elements (Warren, 1996).

Figure 21 shows the variation of the blaze peak efficiency with the deviant angle from the Littrow configuration for the two gratings of IRCS. The diffraction efficiency at the blaze peak decreases with $\cos\alpha/\cos\beta$ (see § 3.6), getting steeper as the blaze angle of the grating increases. The cross-disperser shows about 90 % of efficiency and the echelle shows about 75% of efficiency at the nominal setting.

Although the "off-plane" mount ($\alpha = \beta$, $\gamma \neq 0$) maximizes the blaze peak efficiency because γ is nearly independent of the peak efficiency (see. §3.6), the IRCS echelle is used "in-plane" mount ($\gamma = 0°$) because of the following merits:

1. In-plane mount makes the distribution of intensity more uniform across the entire wavelength range in each order spectrum due to the flatter blaze function. Such uniformity is important to minimize problems caused by the large contrast of spectral lines over a wide wavelength range. For example, such uniformity requires only small dynamic range of the detector for flat fielding. It makes comparatively uniform signal-to-noise ratio over the observed wavelength range.

2. In-plane mount can avoid complication caused by the variable tilt of spectral lines which occur when $\gamma \neq 0$. Such tilts make data reduction process complicated.

40
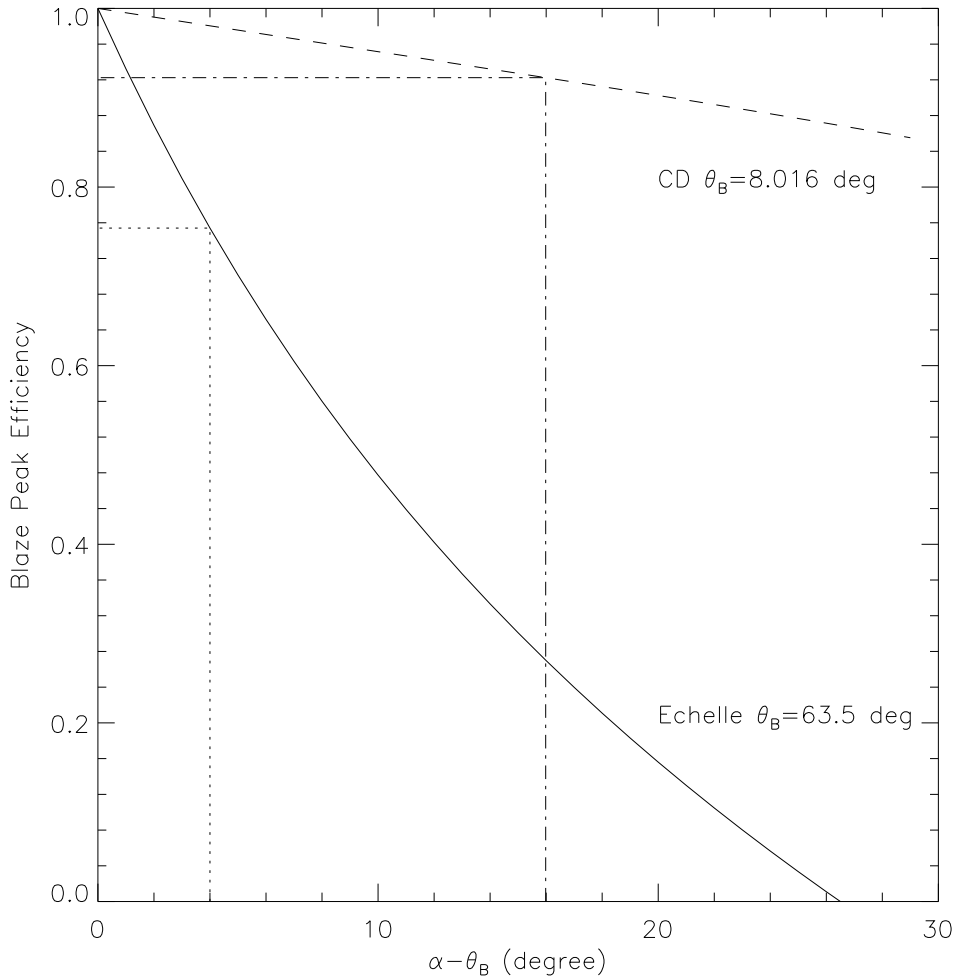
Figure 21: Variation of the blaze efficiency with the difference between the incident and blaze angles, $\alpha - \theta_B$, or the deviant angle from the Littrow Configuration. The solid line is for the echelle grating ($\theta_B = 63°5$) and the dashed line is for the cross-disperser grating ($\theta_B = 8°016$) of IRCS. The dotted and dashed-dotted lines indicate the initial reference angle between the incident and blaze angles for the echelle grating, 4°, and for the cross-disperser, 15°984, respectively.

4.3　Echelle Simulator for IRCS

An Echelle simulator for IRCS was developed by using the equations in § 3.

The purposes of the echelle simulator can be enumerated as follows:

1. It helps users to find the most suitable positions of spectral lines of their interest by adjusting the echelle and cross-disperser setting parameters to avoid bad pixels on the detector.

2. It helps users to identify the spectral features, telluric absorption lines, OH emission lines, stellar photospheric lines, etc. This function is useful for identification of comparison lines as the first step of wavelength calibration.

3. It helps spectrograph developers to predict the spectral format of the echelle spectrograph and to investigate the optical arrangement.

The echelle simulator for IRCS has the following functions in order to make easy comparison between the simulated echellogram and observed frames,

1. The echellogram can be overlapped on an observed frame.

2. It calculates and draws slit images of spectral lines given in a list file.

3. It draws instrumental response functions including the blaze function of the gratings, atmospheric transmittance, and filter transmittance function.

4. It gives a list file for the positions and information of spectral lines.

5. It can draw the atmospheric transmittance overlapped on an observed spectral format.

Figure 22 shows an observed $H-$band frame of the L1551 IRS 5 jet as a background image and indicates OH lines, [Fe II] lines, and atomic hydrogen lines on it. Figure 23 shows a response function including the blaze functions, atmospheric transmittance, and filter transmittance for Figure 22. Table 2 shows data of the spectral lines displayed on Figures 22 and 23.
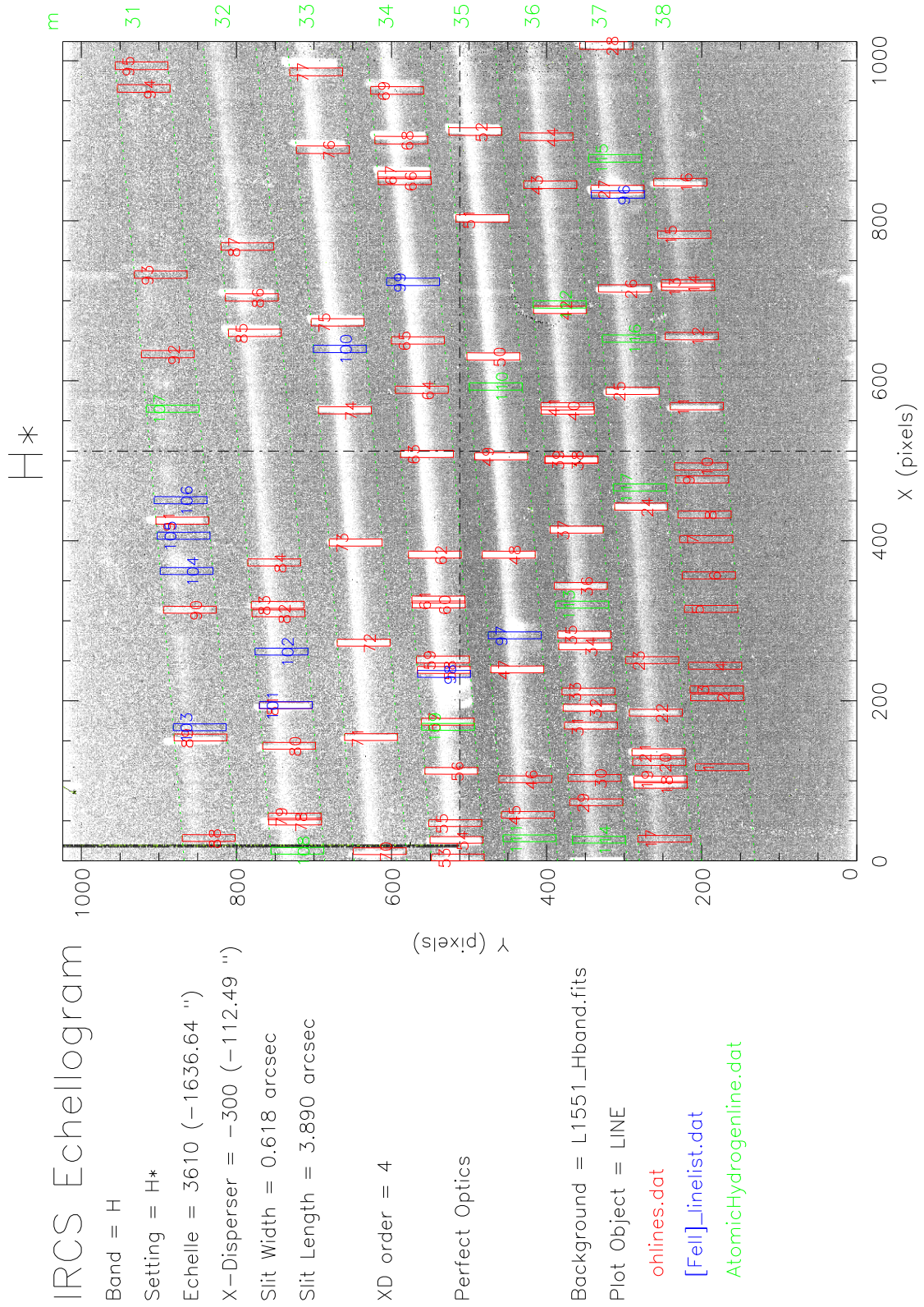
Figure 22: Echelle simulator example for IRCS. An H−band spectral frame of the L1551 IRS 5 jet and OH lines, [Fe II] lines, and atomic hydrogen lines on it.

Figure 23: Response functions of apertures in Figure 22. Solid lines represent product of the blaze functions of the gratings, atmospheric transmittance, and filter transmittance. Red, blue, and green dashed lines indicate the positions of OH emission lines, [Fe II] lines, and atomic hydrogen lines, respectively.

Table 2: List of spectral lines displayed on Figures 22 and 23.

Line Number	Order	Wavelength (μm)	Intensity[†]	Label	X(pixels)	Y(pixels)
1	38	1.46651	0.14	1	116.856	173.867
2	38	1.46984	0.35	2	204.243	179.967
3	38	1.47022	0.01	3	214.277	180.672
4	38	1.47133	0.01	4	243.662	182.746
5	38	1.47400	0.10	5	314.817	187.807
6	38	1.47556	0.05	6	356.704	190.812
7	38	1.47724	0.15	7	402.081	194.090
8	38	1.47837	0.15	8	432.762	196.319
9	38	1.47998	0.30	9	476.699	199.530
10	38	1.48057	0.26	10	492.871	200.717
11	38	1.48330	0.62	11	568.175	206.284
12	38	1.48644	0.20	12	655.815	212.841
13	38	1.48862	0.01	13	717.332	217.495
14	38	1.48877	0.78	14	721.585	217.818
15	38	1.49091	0.10	15	782.571	222.476
16	38	1.49319	0.26	16	848.183	227.534
17	37	1.50261	0.01	17	27.515	247.967
18	37	1.50528	0.01	18	94.896	252.715
19	37	1.50555	1.95	19	101.740	253.200
20	37	1.50640	0.01	20	123.329	254.734
21	37	1.50689	0.66	21	135.801	255.622
22	37	1.50882	0.23	22	185.112	259.152
23	37	1.51137	0.10	23	250.753	263.895
24	37	1.51870	0.38	24	442.678	278.042
25	37	1.52410	1.41	25	587.394	288.988
26	37	1.52878	0.58	26	715.317	298.862
27	37	1.53324	1.15	27	839.558	308.631
28	37	1.53953	0.40	28	1018.979	323.048
29	36	1.54621	0.10	29	73.144	335.853
30	36	1.54744	0.01	30	103.448	338.054
31	36	1.55008	0.20	31	168.878	342.843
32	36	1.55098	0.25	32	191.308	344.496
33	36	1.55179	0.20	33	211.552	345.994
34	36	1.55404	0.55	34	268.063	350.199
35	36	1.55462	0.01	35	282.696	351.294
36	36	1.55702	0.15	36	343.565	355.875
37	36	1.55977	0.70	37	413.926	361.225
38	36	1.56313	0.01	38	500.829	367.913
39	36	1.56316	0.35	39	501.610	367.974
40	36	1.56550	1.05	40	562.778	372.735
41	36	1.56570	0.01	41	568.031	373.146
42	36	1.57025	0.28	42	688.626	382.669
43	36	1.57603	0.10	43	845.031	395.272
44	36	1.57821	0.15	44	905.014	400.182
45	35	1.58973	0.10	45	57.445	424.085
46	35	1.59159	0.01	46	101.946	427.401
47	35	1.59726	0.50	47	239.170	437.776
48	35	1.60308	1.53	48	382.625	448.866
49	35	1.60798	0.65	49	505.619	458.570
50	35	1.61286	1.71	50	630.269	468.592
51	35	1.61947	0.63	51	802.851	482.776
52	35	1.62354	1.27	52	911.426	491.883
53	34	1.63418	0.12	53	4.151	514.548
54	34	1.63513	0.65	54	26.058	516.209
55	34	1.63604	0.10	55	47.095	517.809
56	34	1.63885	0.25	56	112.405	522.813
57	34	1.64147	0.20	57	173.783	527.565
58	34	1.64421	0.01	58	238.497	532.624
59	34	1.64476	0.70	59	251.555	533.651
60	34	1.64764	0.01	60	320.287	539.093
61	34	1.64790	0.50	61	326.523	539.590
62	34	1.65023	0.75	62	382.646	544.081
63	34	1.65539	0.30	63	508.484	554.294
64	34	1.65863	0.01	64	588.657	560.903
65	34	1.66110	0.10	65	650.406	566.048

Table 2: List of spectral lines displayed on Figures 22 and 23.

66	34	1.66892	0.01		66	849.749	582.978
67	34	1.66921	2.30		67	857.260	583.626
68	34	1.67088	0.83		68	900.690	587.384
69	34	1.67325	0.30		69	962.833	592.801
70	33	1.68405	0.30		70	11.966	615.174
71	33	1.69037	1.45		71	154.598	626.430
72	33	1.69551	0.52		72	272.538	635.933
73	33	1.70088	1.80		73	397.750	646.216
74	33	1.70783	0.70		74	563.063	660.100
75	33	1.71236	1.20		75	672.954	669.522
76	33	1.72104	0.36		76	888.728	688.472
77	33	1.72486	0.70		77	986.036	697.212
78	32	1.73838	0.40		78	49.003	724.352
79	32	1.73867	0.40		79	55.322	724.863
80	32	1.74270	0.30		80	143.698	732.068
81	32	1.74499	0.72		81	194.359	736.245
82	32	1.75013	0.27		82	309.296	745.846
83	32	1.75060	0.08		83	319.893	746.740
84	32	1.75294	0.08		84	372.877	751.232
85	32	1.76532	2.00		85	659.895	776.208
86	32	1.76718	0.70		86	704.066	780.148
87	32	1.76984	0.18		87	767.746	785.874
88	31	1.79348	0.05		88	28.408	835.695
89	31	1.79940	1.42		89	154.040	846.248
90	31	1.80679	0.18		90	313.754	859.973
91	31	1.81185	0.50		91	425.095	869.747
92	31	1.82110	0.01		92	633.216	888.469
93	31	1.82542	0.05		93	732.613	897.618
94	31	1.83528	0.01		94	965.302	919.564
95	31	1.83646	0.01		95	993.727	922.295
96	37	1.53300	2.44-3	4F(9/2)-4D(5/2)	832.811	308.096
97	35	1.59900	3.28-3	4F(7/2)-4D(3/2)	281.774	441.044
98	34	1.64400	4.65-3	4F(9/2)-4D(7/2)	233.524	532.234
99	34	1.66400	3.73-3	4F(5/2)-4D(1/2)	723.632	572.210
100	33	1.71100	9.20-4	4F(5/2)-4D(3/2)	639.776	666.661
101	32	1.74500	1.95-3	4F(3/2)-4D(1/2)	194.584	736.263
102	32	1.74800	1.92-3	4D(7/2)-4P(3/2)	261.458	741.829
103	31	1.80000	1.43-3	4F(5/2)-4D(5/2)	166.888	847.339
104	31	1.80900	1.03-3	4F(7/2)-4D(7/2)	362.179	864.203
105	31	1.81100	1.84-3	4D(7/2)-4P(5/2)	406.274	868.083
106	31	1.81300	2.34-3	4D(5/2)-4P(1/2)	450.640	872.013
107	31	1.81810	0.0126	Br(9-4)	565.039	882.271
108	32	1.73670	0.00909	Br(10-4)	12.476	721.407
109	34	1.64120	0.00521	Br(12-4)	167.441	527.071
110	35	1.61140	0.00409	Br(13-4)	592.743	465.555
111	35	1.58850	0.00327	Br(14-4)	28.150	421.915
112	36	1.57050	0.00266	Br(15-4)	695.318	383.202
113	36	1.55610	0.00220	Br(16-4)	320.176	354.110
114	36	1.54430	0.00184	Br(17-4)	26.316	332.472
115	37	1.53460	0.00156	Br(18-4)	877.920	311.682
116	37	1.52650	0.00133	Br(19-4)	652.698	294.005
117	37	1.51960	0.00116	Br(20-4)	466.597	279.835
							(end)

† The values in this column mean as follows: intensities in kR for OH lines (Steed & Baker, 1979), Einstein coefficients for [Fe II] lines (Nussbaumer & Storey, 1988), and relative intensities of I(line)/I(Hβ) (Hummer & Storey, 1987).

46

4.3.1 *Optical parameters obtained by echelle simulator*

The optical parameters of the echelle spectrograph are adjusted by comparing a real spectral format with a simulated one. Table 3 shows the several parameters.

Table 3: Optical parameters of the IRCS echelle spectrograph

Telescope		
Focal length (f_{tel}; mm)	100040	
Aperture (D_{tel}; mm)	8082	
Plate Scale (arcsec mm^{-1})	2.062	
Collimator		
Focal length (f_{col}; mm)	300.00	[320.248]
Aperture (D_{col}; mm)	25.882	
Camera		
Focal length (f_{cam}; mm)	318.0	[315.386]
Aperture (D_{cam}; mm)	34.327	
Detector		
Type	Raytheon InSb Array	
Multiplexer	Aladdin II	
Pixel size (mm pix^{-1})	0.027	
Echelle grating		
Groove spacing (σ_e; mm)	1.0/31.6	
Groove Angle ($\theta_B e$; degree)	63.5	[63.52]
Grating operating angle($(\alpha - \beta)_{e0}$; degree)	8.0	
Cross-Disperser		
Groove spacing (σ_c; mm)	1.0 / 42.5	[1.0/42.35]
Groove Angle ($\theta_B c$; degree)	8.016	
Grating operating angle($(\alpha - \beta)_{c0}$; degree)	31.34498	

* The values in [ ] are original optical design values of IRCS (Warren, 1996).

4.3.2 Setting parameters of the echelle and cross-disperser

The setting parameters of the echelle (ESP) and cross-disperser (XSP) gratings are related to the offset angles from the nominal setting with $\alpha_e = 67°\!.5$ and $\alpha_c = 24°\!.0$ for the echelle and cross-disperser, respectively. The ESP and XSP are input parameters on GUI for controlling of IRCS. The offset angles are find by fitting the positions of comparison lines on between observational data and calculated data with the Echelle simulator for IRCS. Eqs. 42 and 43 show the relations between the offset angles and ESP or XSP, which are as follows

$$\delta\alpha_e = (-1.2751 \pm 0.0019)\text{ESP} + (3026.47 \pm 12.30), \tag{42}$$

$$\delta\alpha_c = (1.0383 \pm 0.0044)\text{XSP} + (159.00 \pm 14.41). \tag{43}$$

Figures 24 and 25 show the relations and residuals. The standard deviations of the residuals are about 40 arcseconds. The mismatches are within 10 pixels for the position of the spectral lines.
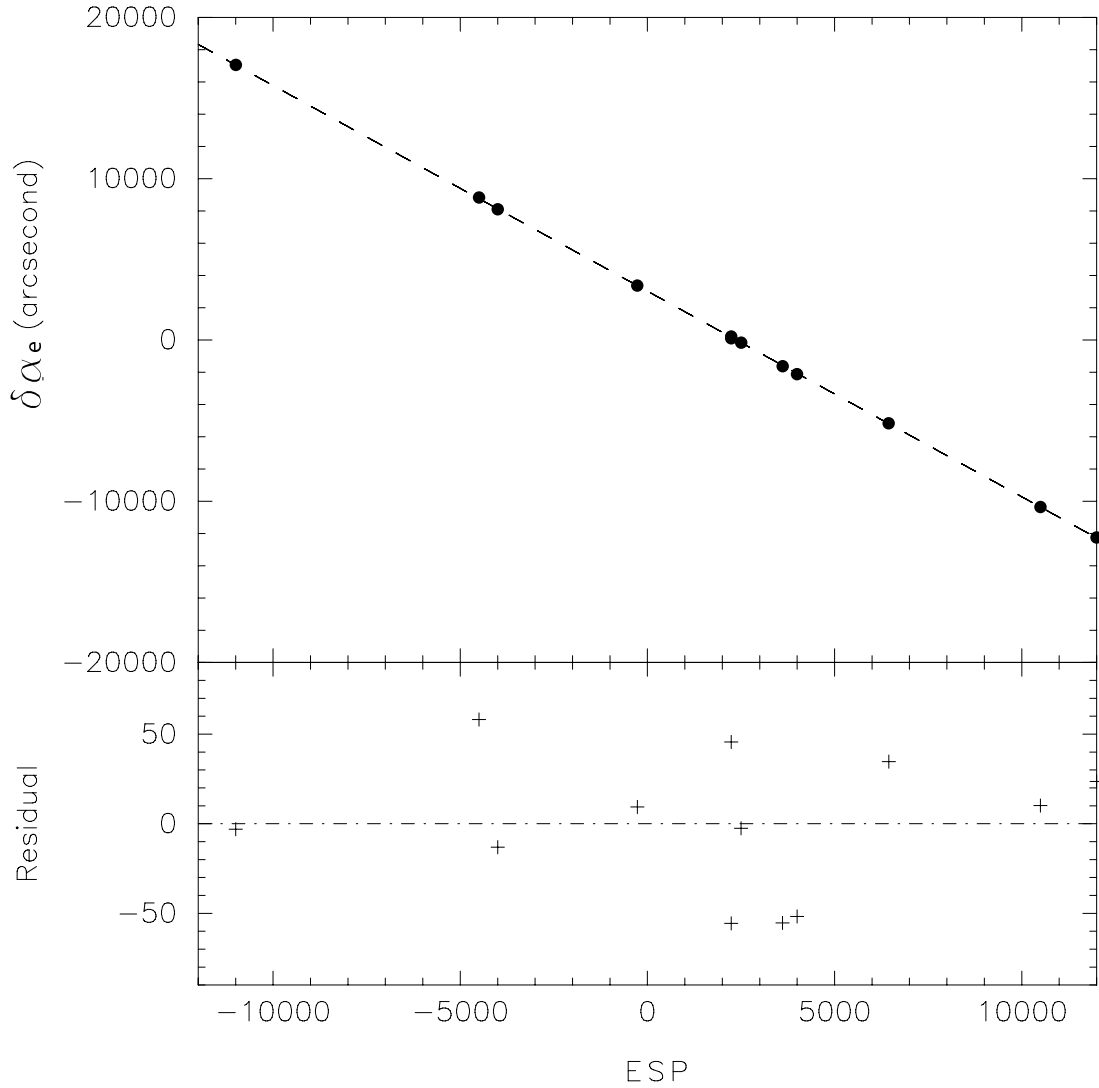
Figure 24: Relation between the echelle setting parameters (ESP) and offset angles from the nominal incident angle ($\alpha = 67^\circ.5$). The lower panel shows the residuals after subtracting the offset angles of Eq. 42 obtainded by a least square fitting from measured offset angles.
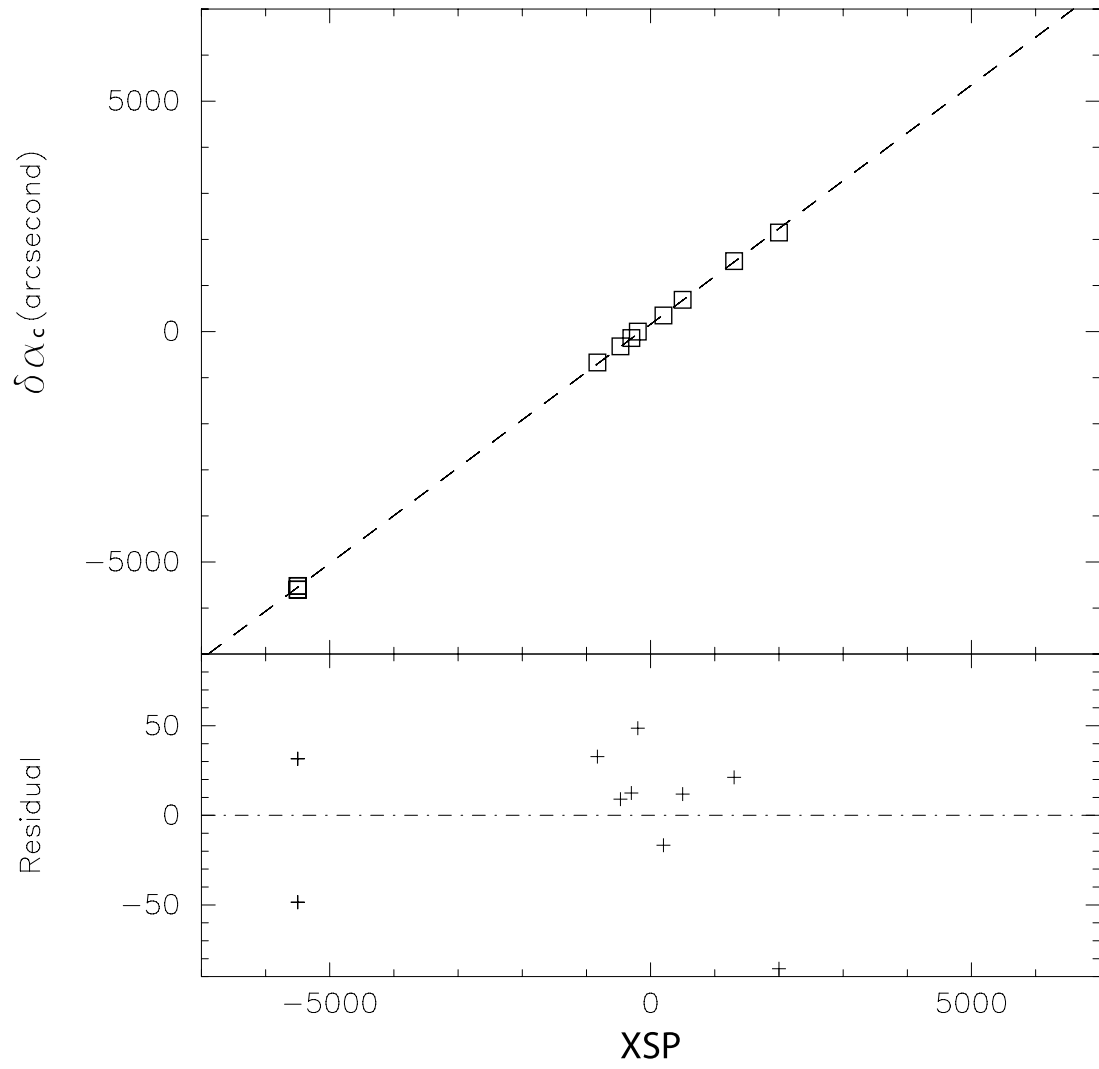
Figure 25: Relation between the cross-disperser setting parameters (XSP) and offset angles from the nominal incident angle ($\alpha = 24\overset{\circ}{.}0$). The lower panel shows the residuals after subtracting the offset angles of Eq. 43 obtainded by a least square fitting from measured offset angles.

4.3.3 *Atmospheric transmittance, filter response functions, and blaze functions*

Figure 26 shows atmospheric transmittance from 1.0 μm to 5.5 μm, response functions of the order sort filters, and blaze functions of the echelle and cross-disperser gratings.

The atmospheric transmittance for the Mauna Kea summit was calculated from 1.0 μm to 5.5 μm by 'ATRAN' program of Load (1992). The blaze function depends on the incident angle toward the grating. Figure 26 c and d show the blaze functions at the nominal setting angle, $\alpha_e = 67\overset{\circ}{.}5$ and $\alpha_c = 24\overset{\circ}{.}0$ for the echelle and cross-disperser, respectively.
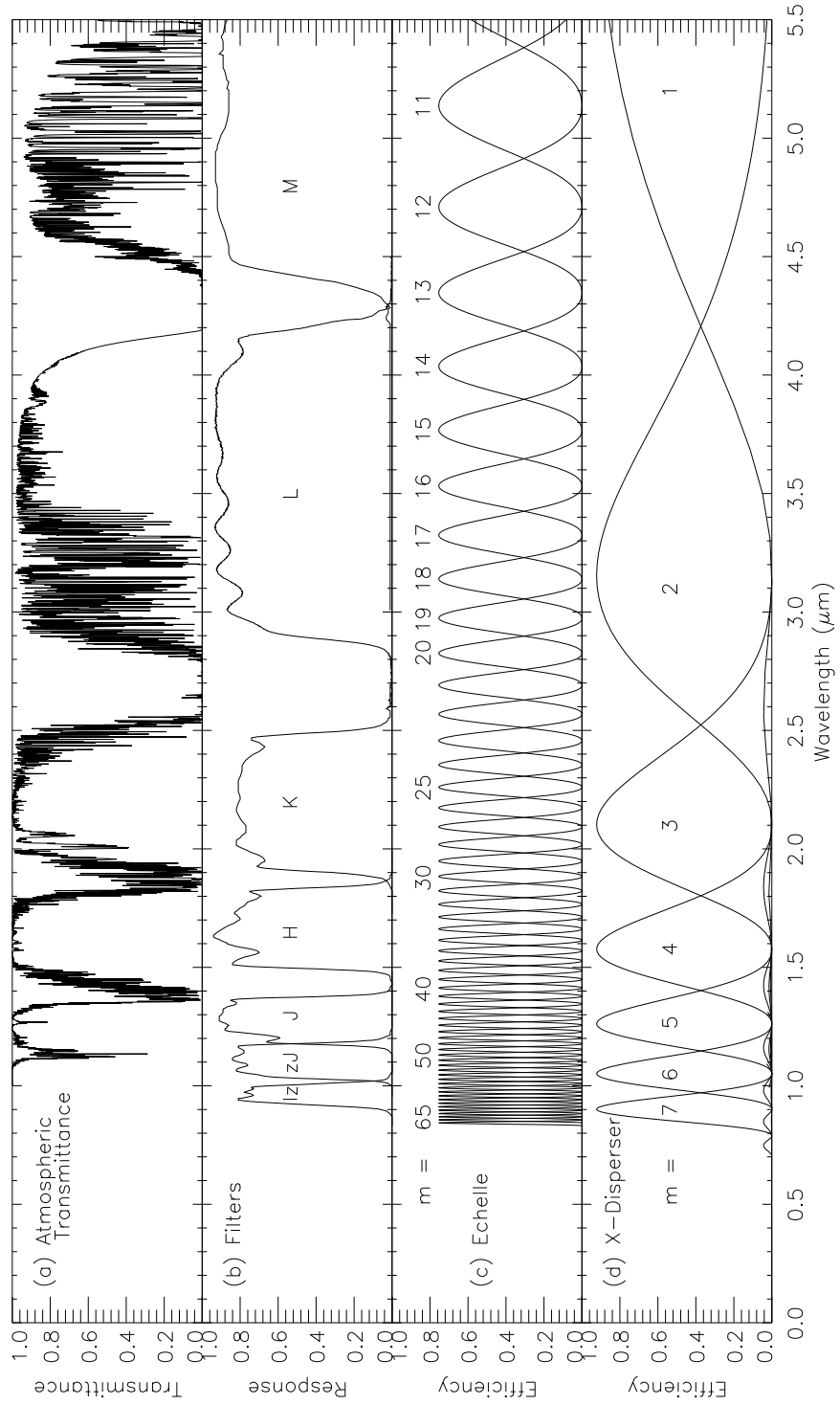
Figure 26: Atmospheric transmittance, response function of the order sort filters, and blaze functions of the echelle and cross-disperser gratings.

5 DATA REDUCTION OF ECHELLE SPECTRA

This section describes the procedure to make a position-velocity diagram at a specific wavelength of the echelle spectrum in order to derive the spatial information along the slit. For this purpose, firstly, the spectrum of each order is traced and then extracted as a spectrum preserved its positional information along the slit length. The curvature and inclination of the spectra are corrected. Secondly, the curvature and inclination of slit images are corrected and the wavelength is calibrated for each two-dimensional image.

The data reduction was performed with the Image Reduction Analysis Facility (IRAF). General reduction procedure of spectra with IRAF was introduced in several documentations (Willmarth & Barnes, 1994; Massey, Valdes, & Barnes, 1992; Valdes, 1986).

5.1 Preparation of Data Reduction

The data reduction of echelle spectra is performed mainly with the tasks of *noao.imred.echelle* and *noao.twodspec.longslit* packages. Before starting the data reduction with the IRCS echelle data, one has to investigate the aperture width, intensity level, dispersion direction, interval between apertures, etc., and then sets the parameters as in Figure 27.

```
noao.imred.echelle        ; call the echelle package to use
echelle.dispaxis = 1      ; set dispersion axis as X-axis
apedit.width = 70         ; set aperture width (~ (slit length)/(pixel scale))
apedit.radius = 35        ; set radius to calculate the center of the aperture
                            ( < apedit.width / 2)
apfind.minsep=75          ; set minimum separation between the apertures
apresize.ylevel = 0.1     ; set intensity level to resize the aperture width
apresize.peak = yes       ; set the above ylevel as a fraction of the peak

noao.twodspec.longslit    ; call the longslit package to use
longslit.dispaxis = 1     ; set dispersion axis as X-axis
```

Figure 27: Setting basic parameters for IRCS echelle spectra when the slit length is $3''\!.89$. The pixel scale of the echelle spectra along the slit length is about $0''\!.060$.

5.2 Dark Subtraction

Dark current arises mainly from the thermal electrons produced in electronic circuits including thermal noise from devices surrounding the detector. The dark current increases with the integration time. Dark frames must be obtained with the same integration time, non-destructive read-out number, and co-add number as the object frame when the dome

and primary mirror cover of the telescope are closed. A reference dark frame is made of combining several dark frames with median filtering in order to exclude cosmic ray events. Figure 28 show a reference dark frame. Dark current is subtracted from each object frame by using the reference dark frame.
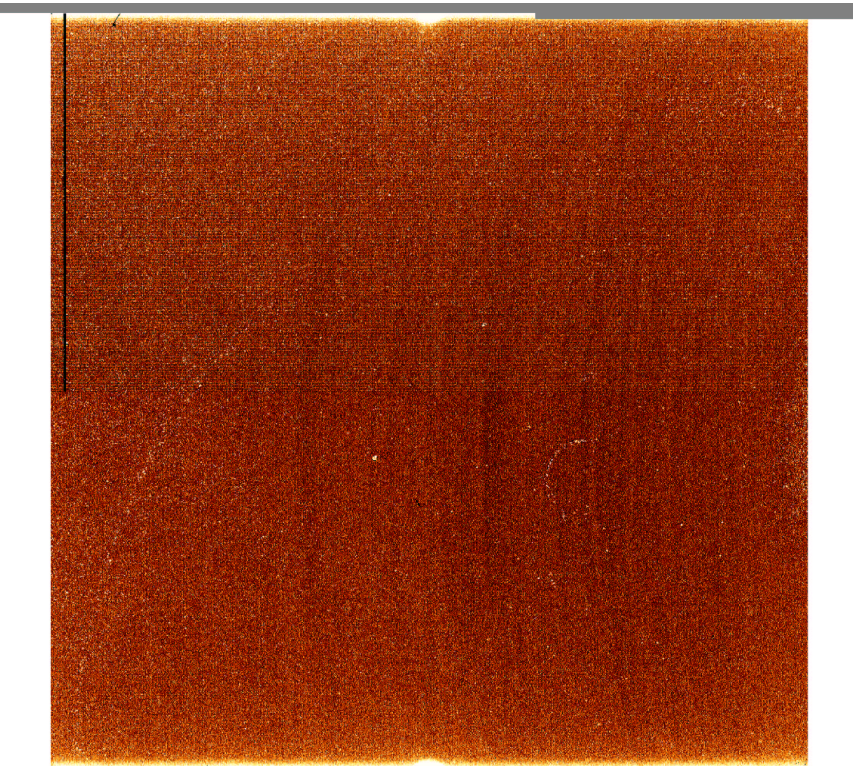
Figure 28: A reference dark frame made of combining several dark frames with median filtering. The integration time is 300 s.

5.3   Flat Fielding

All observed frames must be divided by a normalized flat frame in order to correct the sensitivity difference among detector pixels. This procedure is called the *flat fielding*. Flat frames are obtained by subtracting median OFF-flat frame from median ON-flat frame. While OFF-flat frames are taken when the continuum light source is turned off, ON-flat frames are taken when the light source is turned on with a uniform brightness distribution. The OFF-flat frames include background thermal noise and dark noise. The ON-flat frames must have sufficient intensity level with a high signal-to-noise ratio. Median OFF- and ON-flat frames are made of combining several frames with median filtering to exclude cosmic ray events and reduces noise. Figures 29 and 30 show the median OFF- and ON-flat frames of H and K bands. The background thermal noise, which is more dominant in $K-$band, and dark noise are excluded by subtraction median OFF-flat frame from median ON-flat frame.

For image frames, the flat fielding is completed by dividing object frames by the median flat frame. For spectral frames, however, one has to proceed further in order to make a flat frame due to the following reasons.

1. Spectral frames have inter-order regions where the light from the light source does not arrive except for scattering light or ghosts. The pixel values of such regions are generally low. These regions would have very large pixel values close to infinity if the flat fielding is done using a median flat frame. In order to avoid this, inter-order regions in flat frames must be set to unity.

2. The median flat frame has an illumination profile along the wavelength reflecting the characteristics of the lamp (temperature, spectral lines, etc.). The illumination profile must be removed by fitting a proper polynomial to the median flat frame.

3. The illumination profile along the wavelength also varies with the blaze functions of the echelle and the cross-disperser. The blaze functions are removed from the median flat frame by fitting polynomials.

The next subsections explain these procedure in detail.
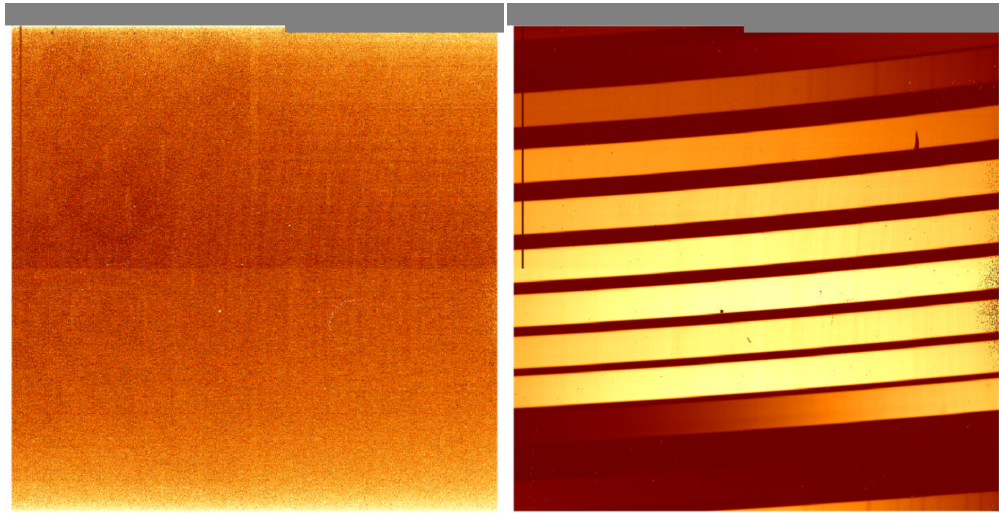
Figure 29: Frames for making $H-$band flat frame. (*left*) OFF flat frame and (*right*) ON flat frame.
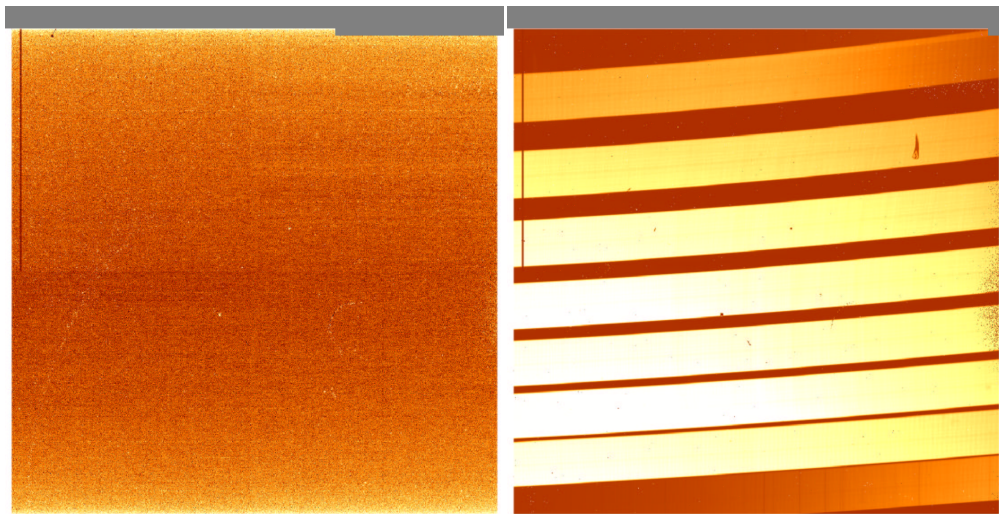
Figure 30: Frames for making $K-$band flat frame. (*left*) OFF flat frame and (*right*) ON flat frame.

5.3.1 *Make aperture trace information with standard star frames*

Spectra of a standard star or a point source are used to trace the aperture on the detector array. APALL task is used for tracing and extracting apertures (Massey, Valdes, & Barnes, 1992). The traced data is saved in a 'database' directory and referred for setting 'references' parameters of each task. Figure 31 shows an example of a setting of several main parameters necessary to trace apertures of point source spectra. In order to check whether the trace is done successfully, apertures are extracted as images by setting the "strip" for the 'format' option of the APALL and then checked whether the continuum of a standard star or a point source is a straight line with the same Y coordinates such as upper image shown in Figure 44. If the trace is done satisfactory, the frame used by the APALL task can be set as a reference frame. The trace data, then, is applied to the median flat frame by setting the frame name for the 'references' parameter. At this point, the widths of apertures should be adjusted to fit the widths of the entire slit length if the apertures were traced by using a narrow width around the continuum peak of a point source. Figure 32 shows an example setting of several main parameters of the APALL task to adjust the width of apertures.

5.3.2 *Make a normalized flat frame*

The APNORMALIZE or APFLATTEN tasks can be used to make a normalized flat frame in IRAF. Both tasks replace all pixel values outside the apertures by unity. While the APNORMALIZE task simply normalizes the illumination profiles along the dispersion direction of the echelle retaining the profile shape along the slit length, the APFLATTEN task models the illumination profiles along the direction of the echelle dispersion and the slit length

The APNORMALIZE task simply divides the profile along the slit length by the number of pixels corresponding to the aperture width or the mean value of the central two pixels. The spatial profile along the slit length is retained. The spatial profile for median flat fielding contains intensity variation due to nonuniformity of the slit width. The spatial profile must be retained in the flat frame to calibrate spatial profile in the spectra of objects, sky, standard star, and comparison.

The APFLATTEN task uses 'optimal extraction routine' for extracting the illumination profile to maximize signal-to-noise ratios (Horne, 1986; Marsh, 1989). The optimal extraction algorithm assumes that a spatial profile along the slit length is a smooth function of wavelength and can be modeled as a normalized probability distribution. While this method is ideal for spatially unresolved targets or short slit, it is not appropriate when spatial information along the slit is required or important as for objects with spatially extended emission line regions.

Figures 34 and 35 shows the flat frames made by the APNORMALIZE and APFLATTEN tasks. It is clear in these figures that the APFLATTEN task alters the spatial profiles, but the APNORMALIZE task does not. In addition, the APFLATTEN task

```
         input = "Traceref"  List of input images
         nfind = 8              Number of apertures
       (output = "   ")         List of output spectra
    (apertures = "")            Apertures
       (format = " strip")      Extracted spectra format
   (references = " ")           List of aperture reference images
     (profiles = "")            List of aperture profile images
  (interactive =  yes)          Run task interactively?
         (find =  yes)          Find apertures?
     (recenter =  yes)          Recenter apertures?
       (resize =  yes)          Resize apertures?
         (edit =  yes)          Edit apertures?
        (trace =  yes)          Trace apertures?
     (fittrace =  yes)          Fit the traced points interactively?
      (extract =  yes)          Extract spectra?
       (extras = no)         Extract sky, sigma, etc.?
       (review = yes)           Review extractions?
         (line = 475)           Dispersion line
               ...........

   # APERTURE CENTERING PARAMETERS
        (width = 30.)           Profile centering width
       (radius = 15.)           Profile centering radius
    (threshold =  500.)         Detection threshold for profile centering

   # AUTOMATIC FINDING AND ORDE
       (minsep = 70.)           Minimum separation between spectra
       (maxsep = 200.)          Maximum separation between spectra
               ...........

   # RESIZING PARAMETERS
       (ylevel = 0.1)           Fraction of peak or intensity for automatic width
         (peak =  yes)          Is ylevel a fraction of the peak?
          (bkg =  no)           Subtract background in automatic width?
               ...........
```

Figure 31: Several main parameters of the APALL task to make the aperture data from point source spectra of Traceref.imh. The paremeters with *itelic* are critical.

58

```
> lpar apall

        input = "TraceRef1"       List of input images
        nfind = 8                 Number of apertures to be found automatically
      (output = "  ")             List of output spectra
  (apertures = "")                Apertures
     (format = " strip")           Extracted spectra format
 (references = " TraceRef")       List of aperture reference images
    (profiles = "")               List of aperture profile images
 (interactive =  no)               Run task interactively?
        (find =  no)               Find apertures?
    (recenter =  no)               Recenter apertures?
      (resize = yes)              Resize apertures?
        (edit =  no)               Edit apertures?
       (trace =  no)               Trace apertures?
    (fittrace =  no)               Fit the traced points interactively?
     (extract = yes)              Extract spectra?
      (extras =  no)               Extract sky, sigma, etc.?
      (review =  no)               Review extractions?
    ............
# RESIZING PARAMETERS
      (llimit = -29.)             Lower aperture limit relative to center
      (ulimit = 75.)              Upper aperture limit relative to center
      (ylevel =  INDEF)            Fraction of peak or intensity for automatic width
............
```

Figure 32: Several main parameters of the APALL task to adjust the widths of apertures which are determined by *llimit* and *ulimit*. These limit parameters are adjusted to show all spectrum area along the slit length.

```
> lpar apnormalize

        input = "Flat.imh"      List of images to normalize
       output = "NFlat.imh"     List of output normalized images
  (apertures = "8")             Apertures
 (references = " TraceRef1")     List of reference images
(interactive = yes)            Run task interactively?
       (find =   no)            Find apertures?
   (recenter =   no)            Recenter apertures?
     (resize =   no)            Resize apertures?
       (edit =   no)            Edit apertures?
      (trace =   no)            Trace apertures?
   (fittrace =   no)            Fit traced points interactively?
  (normalize =  yes)             Normalize spectra?
    (fitspec = yes)            Fit normalization spectra interactively?
       (line = 470)            Dispersion line
       (nsum = 30)             Number of dispersion lines to sum or median
    (cennorm = no)             Normalize to the aperture center?
  (threshold = 100.)           Threshold for normalization spectra
 (background = " none")          Background to subtract
    (weights = " none")          Extraction weights (none|variance)
       (pfit = "fit1d")        Profile fitting type (fit1d|fit2d)
      (clean =   no)            Detect and replace bad pixels?
     (skybox = 1)              Box car smoothing length for sky
 (saturation = INDEF)          Saturation level
  (readnoise = "0.")           Read out noise sigma (photons)
       (gain = "1.")           Photon gain (photons/data number)
     (lsigma = 4.)             Lower rejection threshold
     (usigma = 4.)             Upper rejection threshold
   (function = "legendre")     Fitting function for normalization spectra
      (order = 3)              Fitting function order
     (sample = "*")            Sample regions
   (naverage = -1)             Average or median
   (niterate = 5)              Number of rejection iterations
 (low_reject = 3.)             Lower rejection sigma
(high_reject = 3.)             High upper rejection sigma
       (grow = 0.)             Rejection growing radius
       (mode = "ql")
```

Figure 33: A parameter set for the APNORMALIZE task. The parameters with *italic* are critical.

takes the bad pixels or cosmic ray events into account, altering the intensity distribution around these pixels, but the APNORMALIZE task does not.

The large scale curved patterns, or "tree-ring" patterns, seen in Figure 34 and 35 show a characteristic flat-field variation of InSb detectors (McLean, 1997). Figure 35 (a) shows a stripe pattern along the slit length for the entire aperture. This pattern may be due to the nonuniformity of the K-band slit width.

Because we mainly study spatially extended jets, we use the APNORMALIZE task to make a normalized flat frame.

5.3.3 Flat Fielding

For the flat fielding, all frames of objects, sky, standard stars, and comparison are divided by the normalized flat frame.
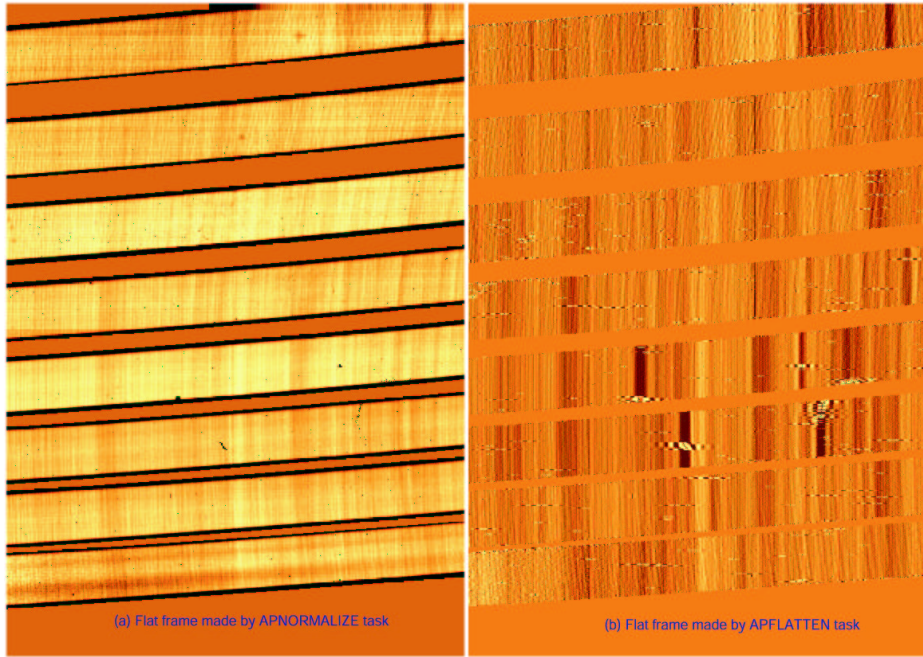
Figure 34: Part of the normalized flat frames of H-band made by (a) APNORMALIZE task (b) APFLATTEN.
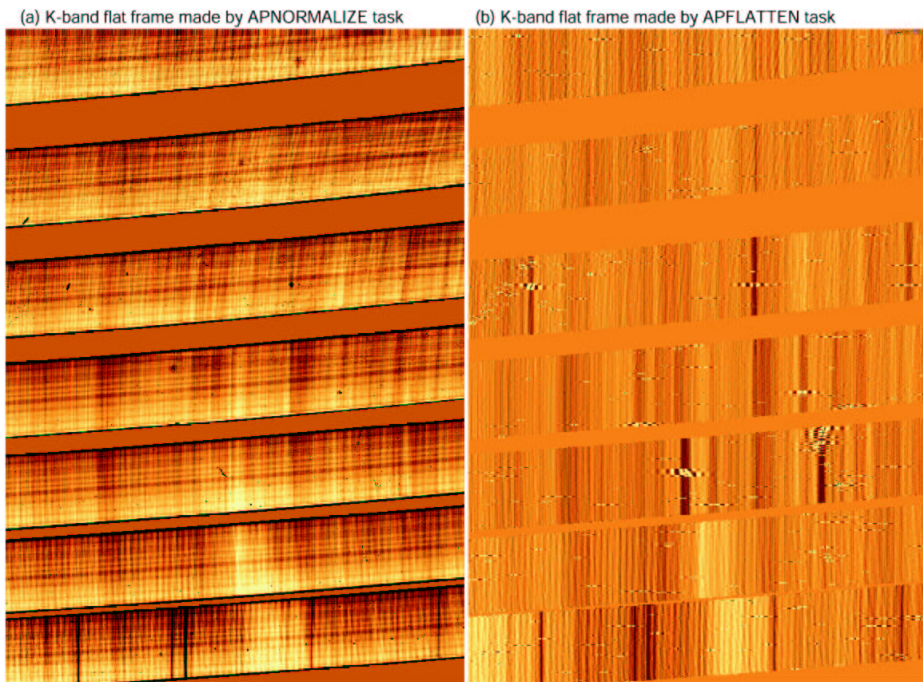
Figure 35: Part of the normalized flat frames of K-band made by (a) APNORMALIZE (b) APFLATTEN.

5.4   Bad Pixel Correction

Usually, a detector array has a few bad pixels which do not have proper working conditions. The detector of the echelle section of IRCS has bad pixels less than ∼0.7 percent. The bad pixel mask was made of replacing the pixel values of dark and normalized flat frames by 1 for bad pixels and 0 for good pixels. Most bad pixels usually have too high or low pixel values, so one can pick them out and replacing their pixel values by using IMREPLACE task with adjusting its 'upper' and 'lower' parameters. Several bad pixels which could not be picked out by IMREPLACE task can be added to the bad pixel image manually with TVMARK, TEXT2MASK, and ADDMASK tasks (see, Figure 36). Figure 37 shows the bad pixels on the detector of the echelle section.

The FIXPIX task is used to correct badpixels.

```
[From flatframe]
imcopy nflatH33.imh H33mask1.imh
imreplace H33mask1 -40000 upper=0.8
imreplace H33mask1 -40000 lower=1.3
imreplace H33mask1 0 lower=-1000
imreplace H33mask1 1 upper=-1000

[Adding bad pixel lines]
imreplace H33mask1[18:21,513:1024] 1.0 lower=INDEF upper=INDEF

[Adding other bad pixels]
display nflatH33.imh 1
tvmark 1 badpixel.coo inter+
 (: Add the coordinates under a cursor with 'a' key,
    save with 'w' key, and quit with 'q'.)
text2mask badpixel.coo badpixel.pl ncol=1024 nlines=1024
addmask H33mask1.imh,badpixel.pl BADPIXEL.imh im1.or.im2

[Correcting bad pixels with the bad pixel mask]
fixpix object.imh BADPIXEL.imh
```

Figure 36: An example procedure for making a bad pixel mask and correcting bad pixels on an object.imh.

Figure 37: Bad pixels on the detector of the echelle section of IRCS. Black dots and lines are the bad pixels.

5.5 Cosmic-ray Events Correction

High energy particles, i.e., *cosmic-rays*, often hit the surface of a detector during integration of a frame. The pixels hit by cosmic-rays have high pixel values. Such cosmic-ray events are corrected by the COSMICRAYS task. This task detects the candidate pixels which exceed mean value of the surrounding pixels within a specified detection window (either 5×5 or 7×7) by the amount specified by the parameter 'threshold'. The COSMICRAYS task replaces the pixel value of the candidate with the average of the four neighbors.

The COSMICRAYS task can be used to remove hot or cool pixels as well as cosmic-ray events. For this purpose, the COSMICRAYS task is applied two times: it is applied to the original frames and to their inverse frames that are the original frames multiplied by −1, and then the inverse frames are recovered to have the signs of the original frames again. Figure 38 shows an example procedure.

```
cosmicrays object.imh cobject.imh
imarith cobject.imh * -1. cobject.imh
cosmicrays cobject.imh cobject.imh
imarith cobject.imh * -1. cobject.imh
```

Figure 38: An example procedure to correct cosmic ray events for an object frame.

5.6 Aperture Extraction

Apertures of all frames are extracted by the APALL task with the median flat frame as a common reference frame. Figure 39 shows the parameter setting as an example.

```
> lpar apall

        input = "@objects.list" List of input images
        nfind = 8               Number of apertures to be found automatically
     (output = "  ")            List of output spectra
  (apertures = "")              Apertures
     (format = " strip")         Extracted spectra format
 (references = " TraceRef1")    List of aperture reference images
   (profiles = "")              List of aperture profile images
(interactive = no)              Run task interactively?
       (find = no)              Find apertures?
   (recenter = no)              Recenter apertures?
     (resize = no)              Resize apertures?
       (edit = no)              Edit apertures?
      (trace = no)              Trace apertures?
   (fittrace = no)              Fit the traced points interactively?
    (extract = yes)             Extract spectra?
     (extras = no)              Extract sky, sigma, etc.?
     (review = no)              Review extractions?
............
```

Figure 39: Main parameters to extract apertures for all frames with a reference frame.

5.7 Wavelength Calibration and Distortion Correction

Wavelength calibration is divided into two steps. The first step is to identify comparison lines which have known wavelengths. From this step one obtains a relation between the pixel number along the dispersion direction and wavelength. This is called the *dispersion solution*. The second step is to convert the non-equal wavelength interval per pixel into 'equal wavelength interval' per pixel and to redistribute the pixel value (flux) along the wavelength by appropriate interpolation. This is called the *linearize*.

Geometrical distortion correction along the spatial direction must also be accomplished. The slit images or monochromatic line images have curvature and inclination as shown in § 3.4. The distortions of images vary with wavelength or pixel number along the dispersion axis (Eq. 17). The relation between the pixel number and distortion can be obtained from the comparison lines. We will call it as the *distortion solution*. The slit images are then corrected to be a straight line perpendicular to the dispersion axis at each wavelength.

Both wavelength calibration and distortion correction can be accomplished *simultaneously* with the *noao.twodspec.longslit* package (Valdes, 1986; Massey, Valdes, & Barnes, 1992). The overall process is as follows:

1. To identify comparison lines along the dispersion direction at the center of the aperture.

2. To measure the distortions along spatial direction for the comparison lines.

3. To determine a two dimensional transformation function between the image coordinates and user coordinates obtained from the dispersion and distortion solutions.

4. To transform the original image into an image with uniform and orthogonal grid in the user coordinates.
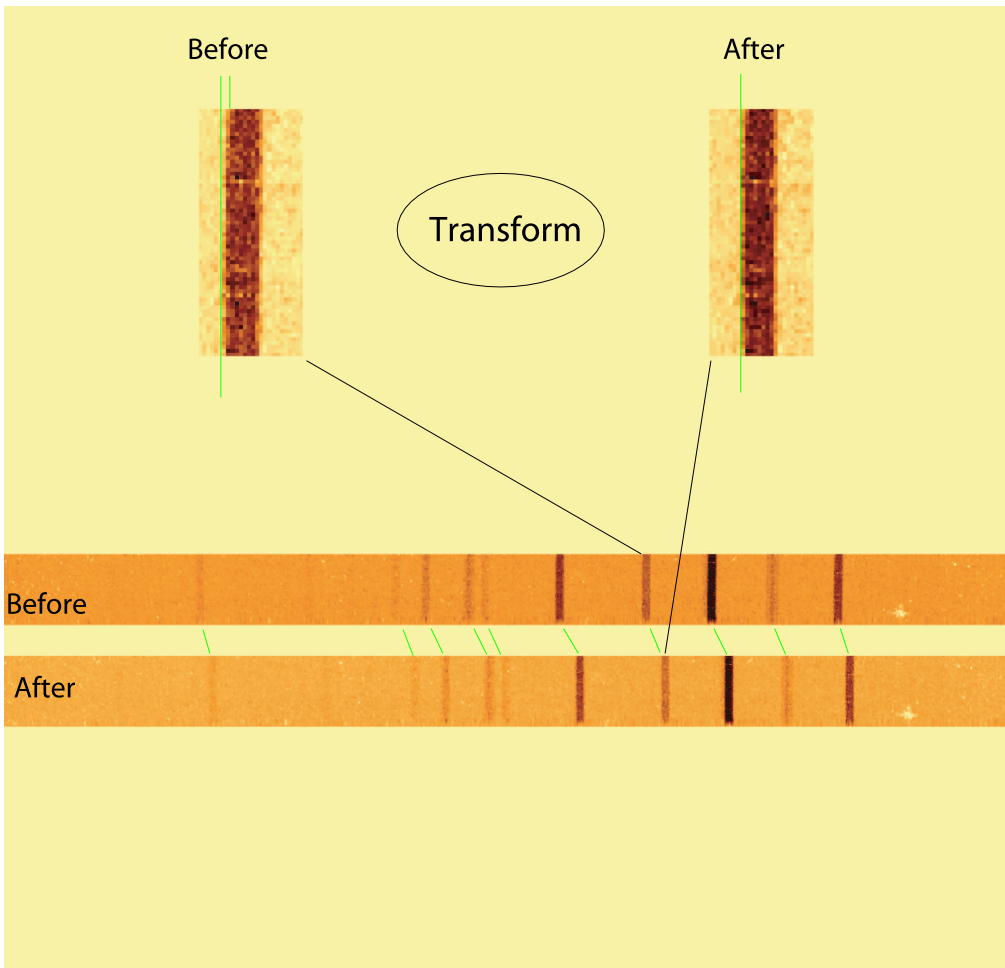
Figure 40: A conceptional diagram of transformation from the image coordinates to the user coordinates during wavelength calibration and distortion correction. This diagram shows *before* and *after* the application of transformation of coordintes. Two images of a comparison line at the upper part show difference between before and after the distortion correction. Two aperture images at lower part show difference between before and after the wavelength calibration.

5.7.1 *Determination of the dispersion solution: the IDENTIFY task*

The IDENTIFY task is used to identify comparison lines in a one-dimensional spectral image and to determine the dispersion solution. The comparison lines must be taken ideally in the same configuration with object frames. The comparison lines can be usually obtained from the calibration lamp emitting Th-Ar lines. In the near infrared J-, H-, and K- bands, there are many OH sky emission-lines and telluric absorption lines (Rousselot et al., 2000; Maihara et al., 1993; Oliva & Origlia, 1992). These lines can be obtained from sky frames taken at positions near the objects or from object frames themselves under the same instrument configurations as those for the object frames. The OH sky emission lines thus offer the best conditions to obtain accurate dispersion solution.

5.7.2 *Determination of the distortion solution: the REIDENTIFY task*

The REIDENTIFY task traces slit images and measure their positions along the spatial direction of the comparison lines which was identified by the IDENTIFY task. This task makes distortion solutions for the comparison lines. Figure 41 shows parameters of the REIDENTIFY task and a result of execution of it.

```
>lpar reidentify
reference = "nvH33_OH.0001" Reference image
        images = "nvH33_OH.0001" Images to be reidentified
        answer = "NO"                  Fit dispersion function interactively?
         crval =                       Approximate coordinate (at reference pixel)
         cdelt =                       Approximate dispersion
 (interactive = "no")            Interactive fitting?
     (section = "middle line")   Section to apply to two dimensional images
       (newaps = yes)            Reidentify apertures in images not in reference?
     (override = yes)            Override previous solutions?
        (refit = yes)            Refit coordinate function?
        (trace = no)             Trace reference image?
         (step = " 10")           Step in lines/columns/bands for tracing an image
         (nsum = "10")           Number of lines/columns/bands to sum
        (shift = "0.")           Shift to add to reference features (INDEF to search)
       (search = 0.)             Search radius
        (nlost = 0)              Maximum number of features which may be lost
      (cradius =  5.)             Centering radius (= width of a spectral line)
    (threshold = 0.)             Feature threshold for centering
  (addfeatures = no)             Add features from a line list?
    (coordlist = "linelists$issac_OHlistv20.dat") User coordinate list
        (match =  -3.)             Coordinate list matching limit
  (maxfeatures = 50)             Maximum number of features for automatic identification
       (minsep = 2.)             Minimum pixel separation
     (database = "database")     Database
     (logfiles = "reidentify.log") List of log files
     (plotfile = "")             Plot file for residuals
      (verbose = yes)            Verbose output?
     (graphics = "stdgraph")     Graphics output device
       (cursor = "")             Graphics cursor input
      (aidpars = "")             Automatic identification algorithm parameters
         (mode = "ql")

>reidentify nvH33_OH.0001  nvH33_OH.0001

REIDENTIFY: NOAO/IRAF V2.11EXPORT pyo@coconut Mon 10:27:31 26-Mar-2001
  Reference image = nvH33_OH.0001, New image = nvH33_OH.0001, Refit = yes
         Image Data     Found    Fit Pix Shift  User Shift  Z Shift     RMS
nvH33_OH.0001[*,26]      8/8     8/8     0.122      0.0457  3.11E-6   0.0659
nvH33_OH.0001[*,26]      8/8     8/8     0.122      0.0457  3.11E-6   0.0659
nvH33_OH.0001[*,16]      8/8     8/8    -0.248     -0.0923  -6.2E-6   0.0883
nvH33_OH.0001[*,6]       8/8     8/8    -0.316      -0.117  -7.9E-6    0.205
nvH33_OH.0001[*,46]      8/8     8/8     0.165      0.0604  4.07E-6   0.0837
nvH33_OH.0001[*,56]      8/8     8/8     0.0806     0.0281  1.89E-6   0.0317
nvH33_OH.0001[*,66]      8/8     8/8     0.356       0.128  8.65E-6   0.0802
```

Figure 41: An example of the parameter setting and execution of the REIDENTIFY task. The parameters in *italic* are critical.

5.7.3 *Making transformation of coordinates: the FITCOORDS task*

The FITCOORDS task determines the user coordinates from the data produced with the IDENTIFY and REIDENTIFY tasks.

The dispersion solution is theoretically represented by Eq. 3 for an ideal case. The transformation function in the dispersion direction (X) can be set to a fourth or fifth order function in IRAF[1].

A slit image is represented by a parabolic function as explained in § 3.4. The transformation function in the spatial direction (Y) can be set to a third order equation or second order equation in IRAF if the curvatures of slit images are negligible.

```
>lpar fitcoord

        images = "nvH33_OH.0001" Images whose coordinates are to be fit
     (fitname = "")                Name for coordinate fit in the database
 (interactive = yes)               Fit coordinates interactively?
     (combine = no)                Combine input coordinates for a single fit?
    (database = "database")        Database
   (deletions = "deletions.db") Deletion list file (not used if null)
    (function = "chebyshev")     Type of fitting function
      (xorder =    4)              X order of fitting function
      (yorder =    3)              Y order of fitting function
    (logfiles = "STDOUT,logfile") Log files
    (plotfile = "plotfile")       Plot log file
    (graphics = "stdgraph")       Graphics output device
      (cursor = "")               Graphics cursor input
        (mode = "ql")

> fitcoord nvH33_OH.0001

NOAO/IRAF V2.11EXPORT pyo@coconut Mon 10:35:39 26-Mar-2001
  Longslit coordinate fit name is nvH33_OH.0001.
  Longslit database is database.
  Features from images:
    nvH33_OH.0001
  Map User coordinates for axis 1 using image features:
  Number of feature coordnates = 126
  Mapping function = chebyshev
    X order = 4
    Y order = 3
  Fitted coordinates at the corners of the images:
    (1, 1) = 14619.95  (1024, 1) = 14992.94
    (1, 71) = 14620.88  (1024, 71) = 14991.41
```

Figure 42: An example of the parameter setting and execution results of the FITCOORDS task.

---

[1]In IRAF, the order of an equation means the number of terms in it.

5.7.4 *Applying the transformation function: the TRANSFORM task*

The TRANSFORM task transforms an original image into a uniform grid image in the user coordinates created by the FITCOORDS task. The wavelength calibartion including *linearize* and distortion correction are achieved simultaneously with this task. Figure 43 shows the parameters of the TRANSFORM task and the results of its execution as an example.

```
> lpar transform

        input = "nvH33_IRS5_pos1.0001" Input images
       output = "tnvH33_IRS5_pos1.0001" Output images
     fitnames = " nvH33_OH.0001" Names of coordinate fits in the database
    (database = "database")      Identify database
  (interptype = "spline3")       Interpolation type
         (x1 = INDEF)            Output starting x coordinate
         (x2 = INDEF)            Output ending x coordinate
         (dx = INDEF)            Output X pixel interval
         (nx = INDEF)            Number of output x pixels
       (xlog = no)               Logarithmic x coordinate?
         (y1 = INDEF)            Output starting y coordinate
         (y2 = INDEF)            Output ending y coordinate
         (dy = INDEF)            Output Y pixel interval
         (ny = INDEF)            Number of output y pixels
       (ylog = no)               Logarithmic y coordinate?
       (flux = yes)              Conserve flux per pixel?
    (logfiles = "STDOUT,logfile") List of log files
       (mode = "ql")

> transform  nvH33_IRS5_pos1.0001  tnvH33_IRS5_pos1.0001  nvH33_OH.0001

AO/IRAF V2.11EXPORT pyo@coconut Fri 14:45:55 23-Mar-2001
  Transform nvH33_IRS5_pos1.0001 to tnvH33_IRS5_pos1.0001.
  Conserve flux per pixel.
  User coordinate transformations:
    nvH33_OH.0001
  Interpolation is spline3.
  Output coordinate parameters are:
    x1 =      14620., x2 =      14993., dx =      0.3646, nx = 1024, xlog = no
    y1 =          1., y2 =          71., dy =          1., ny =   71, ylog = no
```

Figure 43: An example of the parameter setting and execution results of the TRANS-FORM task.

72

5.8 Sky Subtraction

Background emission from the sky have to be subtracted from the spectra of objects and standard stars. This is achieved by subtracting the sky spectrum from the object or standard star frames. The sky frames are usually taken during observational sequence, *object - sky - sky - object*. The sky frames should be taken near the object frames in time because the sky background emission varies with time. Sky subtraction would leave a residual if the spectra of sky and object frames have different background levels. Such a residual can be eliminated by subtracting a scaled sky frame which is an original sky frame multiflied by a factor to scale its intensity level matching the background level of the object frames. Each aperture has a different scaling factor.

If the object is small compared to the slit length, then the sky can be removed by using either side or both sides of the slit image free of object emission. The sky level is used a median value calculated the either or both sides, or straight line connected between the both sides. This can be achieved by BACKGROUND task in the *noao.twodspec.longslit* package. Figure 44 shows an example of sky subtraction from an object frame with the BACKGROUND task. The distortion of the slit image must be corrected before subtraction.

5.9 Wavelength Sensitivity Calibration

The observed spectrum of an object ($S(\lambda)$) is represented as,

$$S(\lambda) = S_o(\lambda)T_a(\lambda)I(\lambda), \tag{44}$$

where $S_o(\lambda)$ is the spectrum of the object, $T_a(\lambda)$ is the atmospheric transmittance, and $I(\lambda)$ is the effective instrumental response including the diffraction efficiencies of gratings and transmittance of optics. In order to extract the spectrum of the object, $T_a(\lambda)$ and $I(\lambda)$ must be corrected.

The observed spectrum of a standard star ($S_s(\lambda)$) is represented as,

$$S_s(\lambda) = S_*(\lambda)T_{a,s}(\lambda)I_s(\lambda), \tag{45}$$

where S_* is the spectrum of the standard star. The spectrum of the standard star is obtained at the same airmass as the objects. Thus one can assume that $T_a(\lambda) = T_{a,s}(\lambda)$ and $I(\lambda) = I_s(\lambda)$.

A-type stars are usually used as standards because they show almost featureless infrared spectra except for hydrogen absorption lines. One can thus assume that the continuum spectra of standard stars can be represented by a black-body spectra $B_{T_{eff}}(\lambda)$ after correcting the features of hydrogen absorption lines. Thus one can obtain the product of $T_a(\lambda)$ and $I_s(\lambda)$ from normalized $S_s(\lambda)/B_{T_{eff}}(\lambda)$.

The spectrum of an object can then be obtained from the following relation

$$S_o(\lambda) = S(\lambda) \cdot \langle \frac{B_{T_{eff}}}{S_s(\lambda)} \rangle. \tag{46}$$
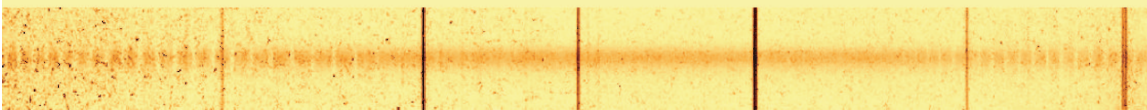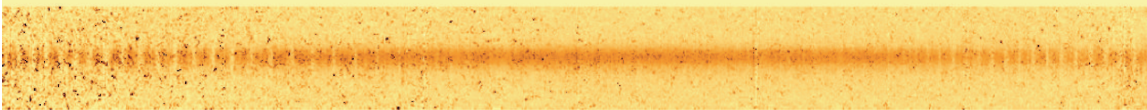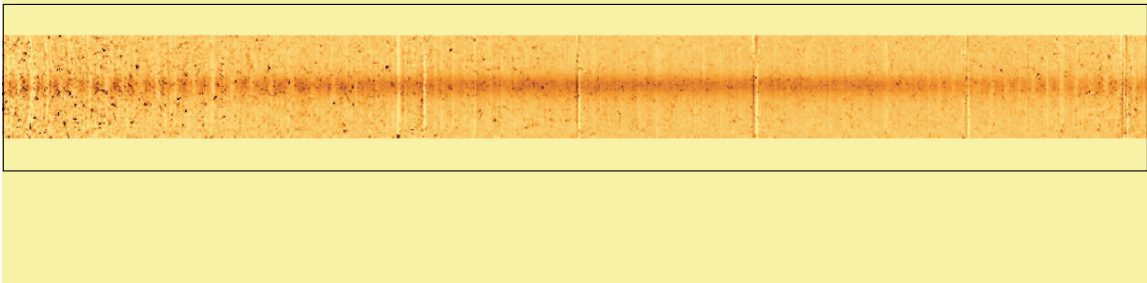
Figure 44: Sky subtraction with the BACKGROUND task. An aperture corrected for its geometrical distortion before (upper image) and after (middle image) the sky subtraction. The lower image in the box is a sky subtracted frame without any distortion correction applied.
.

The details of the procedure are explained below.

5.9.1 *Making frames showing fluxes per unit exposure time*

All object and standard frames, after subtraction of the sky background, must be corrected to have fluxes per unit exposure time before applying the wavelength sensitivity calibration. For this purpose, the frames taken with IRCS have to be divided by $IT \times NDR \times COADD$, where IT is the integration time for each frame, NDR is the number of non-destructive read-out, and $COADD$ is the number of co-adding. These three parameters are shown in the FITS header of each frame as EXP1TIME, NDR, and COADDS, respectively.

5.9.2 *Expanding the spectrum of a standard star along the spatial direction*

The spectrum of a standard star occupies only a narrow part in the spatial direction as the one shown in the upper image of Figure 45. One has to expand the spectrum over the aperture width to correct the wavelength sensitivity for all pixels in the slit length. The procedure to expand the spectrum is shown in Figure 45:

1. A one-dimensional spectrum is made by summing up the standard star flux along the spatial direction (see mean1dspec.cl in Figure 46).

2. Hydrogen absorption lines are removed from the spectrum of the standard star with the SPLOT task as shown Figure 48. Double 'k' keys are used for marking two continuum points and fitting a single Gaussian profile between the two marks. '-' key is used for subtracting the fit.

3. The one-dimensional spectrum is expanded along the spatial direction to have the aperture width (see OneTo2dspec.cl in Figure 47).
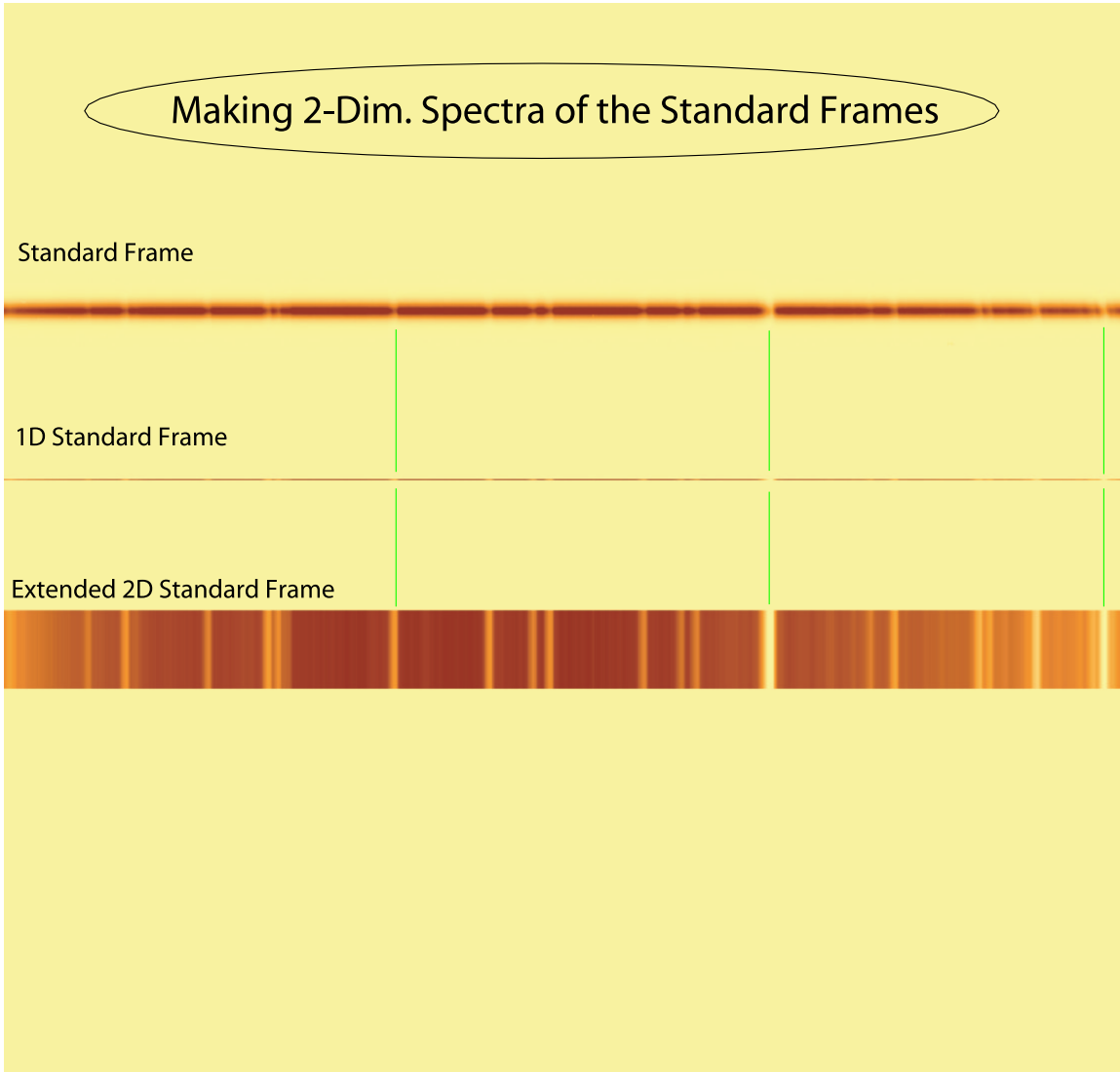
Figure 45: Expanding a standard star spectrum along the spatial direction. An observed spectrum of a standard star subtracted by sky background emission (upper), one-dimensional spectrum made by summing up the standard star intensity distribution along the spatial direction (middle), and the standard star spectrum expanded along the spatial direction (lower).

```
procedure mean1dspec(filename,line1,line2,option)
string filename prompt="INPUT 2D-Spec File"
int line1 prompt="Start line"
int line2 prompt="END line"
string option prompt="average, median, or sum"

begin

    string fname, s1,op
    int l1, l2
    int i

    fname = filename
    l1 = line1
    l2 = line2
    s1 = option

    if(access(fname//".1dlist"))
         del(fname//".1dlist")
    if(access(fname//".imh"))
         for(i=l1; i <=l2; i += 1)
             print(fname//".imh"//"[*,"//i//"]", >> fname//".1dlist")
    if(access(fname//".1d.imh"))
         imdel(fname//".1d.imh")
    if (s1 == "average")
       op = "average"
    else if (s1 == "median")
       op = "median"
    else if (s1 == "sum")
       op = "sum"
    else
      print("Your option of imsum are changed to AVERAGE.")
      op = "average"

      imsum("@"//fname//".1dlist", fname//".1d.imh", option=op)
end

[Usage]
>task mean1dspec = mean1dspec.cl        ; Definition of the task
>mean1dspec std.0001 1 95 sum           ; Makeing 1-D spectra (OUTPUT:*.1d.imh)
```

Figure 46: A CL script to make one-dimensional spectrum and its usage.

```
procedure OneTo2dspec (Onedframe, Twodframe, n)
string Onedframe prompt="1-D spectra"
string Twodframe prompt="2-D spectra expanded"
int    n        prompt="width of the 2-D spectra"

begin
   int nl,i
   string s1
   string s2

   s1 = Onedframe
   s2 = Twodframe
   nl = n

   if(access("1dstack_temp.list"))
      del("1dstack_temp.list")

   for(i=1; i <= nl; i +=1)
      print(s1, >> "1dstack_temp.list")

   if(access(s2//".imh"))
      imdel(s2//".imh")

   imstack("@1dstack_temp.list",s2)
   del("1dstack_temp.list")
end

[Usage]
>task OneTo2dspec = OneTo2dspec.cl        : Definition of the task
>OneTo2dspec std.0001.1d std.0001.2d 70  ; Expand 1-D spectra with width of 70 pixels
```

Figure 47: A CL script to expand one-dimensionl spectrum along the spatial direction
and its usage.

NOAO/IRAF V2.11EXPORT pyo@coconut.subaru.nao.ac.jp Mon 11:11:50 25-Nov-
[Bstd0005.1d.imh]: HD182985 – Aperture 5 60. ap:1 beam:0

NOAO/IRAF V2.11EXPORT pyo@coconut.subaru.nao.ac.jp Mon 11:21:13 25-Nov-
[CBstd0005.1d.imh]: HD182985 – Aperture 5 60. ap:1 beam:0
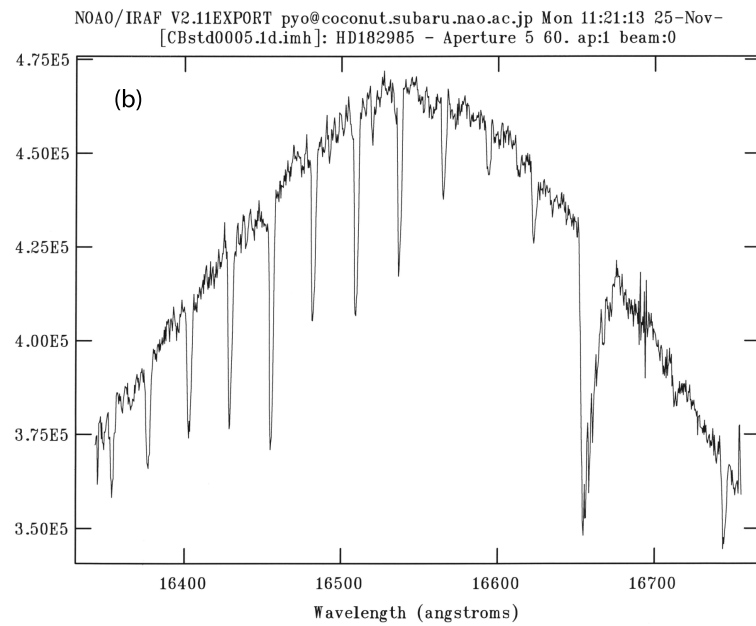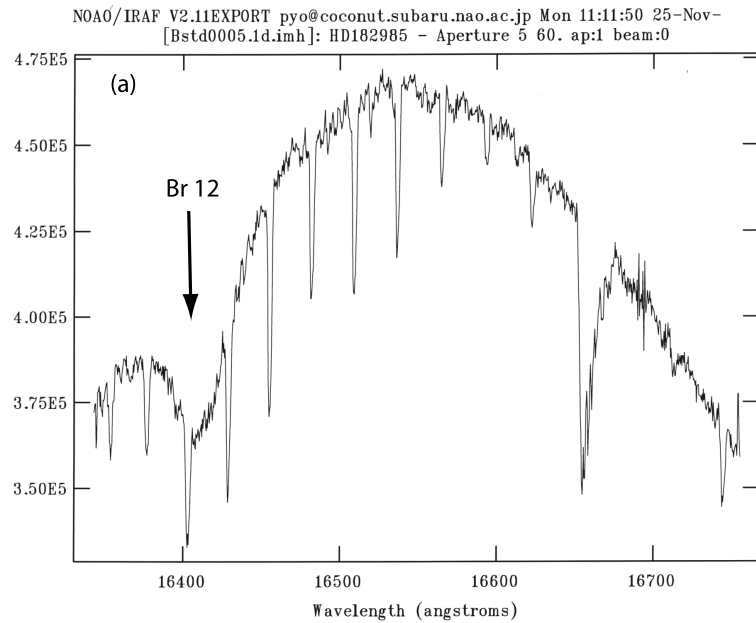
Figure 48: (a) Spectrum of an aperture including the Br12 absorption line. (b) Spectrum after the Br12 absorption line was removed by the SPLOT task.

5.9.3 Making a Blackbody Spectrum

A blackbody spectrum can be made by the MK1DSPEC task in the *noao.artdata* package. Figure 49 shows an example of IRAF script for making a blackbody spectrum with the same temperature as the standard star and the same wavelength range and image size as the aperture.

```
procedure makeBB (imfname,Teff, wlstart, wlend, nc, nl, cont)

string imfname prompt="Output Image Filename"
real    Teff    prompt="Temperature of the Blackbody"
real    wlstart prompt="Start Wavelength"
real    wlend   prompt="End Wavelength"
real    nc      prompt="Number of column(naxis1)"
real    nl      prompt="Number of lines(naxis2)"
real    cont    prompt="Flux at start wavelength"

begin
   real T, ws, we, c
   string s1
   int i, n1, n2

   s1 = imfname
   T = Teff
   ws = wlstart
   we = wlend
   n1 = nc
   n2 = nl
   c  = cont

   unlearn mk1dspec
   mk1dspec(s1, ap = 1, ncols= n1, naps = n2, wstart= ws,
           wend= we, continu= c,tempera= T, comments= yes)
   for(i = 2; i <= n2; i +=1)
      mk1dspec(s1,ap= i, ncols= n1, wstart= ws, wend= we,
               continu= c, tempera= T, comments= no)
   imhead(s1)
end

[Usage]
task makeBB = makeBB.cl            ; Definition of the task

; Standard star = HD25175, V=6.311,A0V, T=9480 K
makeBB BB0005.imh 9480. 16340. 16753. 1024 70 1000.
```

Figure 49: A CL script to make a blackbody spectrum with the same width as the aperture.

5.9.4 *Wavelength Sensitivity Calibration*

A calibration frame for wavelength sensitivity correction is made by normalizing a frame of a blackbody spectrum divided by an expanded standard frame. The wavelength sensitivity calibration is achieved by multiplying an object spectrum with the calibration frame.

5.10 Flux Calibration

Photometric standard stars of known magnitudes at observed wavelengths can be used to calibrate the flux of an object spectrum. When one knows the visual magnitude (V) of a A0 type standard star, the flux of the object can be calibrated by the following steps.

First, calculate flux density at 0.5556 μm (F_V) of the standard star from its V-band magnitude (V),

$$F_{\mathrm{V}} = F_{\mathrm{V,o}} \cdot 10^{-0.4\mathrm{V}}, \tag{47}$$

where $F_{\mathrm{V,o}}$ is the flux density at $V = 0$ mag ($= 3.44\text{E-}08$ W m^{-2} μm^{-1}; Tokunaga (2000)).

Second, calculate flux density at λ μm (F_λ) of the standard star as follows,

$$F_\lambda = B_{T_{eff}}(\lambda) \cdot \frac{F_V}{B_{T_{eff}}(\lambda = 0.5556 \mu m)}. \tag{48}$$

Third, calculate a scaling factor by dividing the spectrum by the standard star spectrum corrected for their wavelength sensitivity.

Fourth, calibrate the flux of the object spectrum by multiplying the scaling factor.

Figure 50 shows example frames of calibrated apertures. If H magnitude of the standard star is known, $F_{\mathrm{H,o}}$ at 1.644 μm and F_{H} must be better for H-band flux calibration. The effective temperature of A0 type star is 9480 K. When the standard star is not A0 type star, the effective temperature depends on their color index (see Tokunaga, 2000).
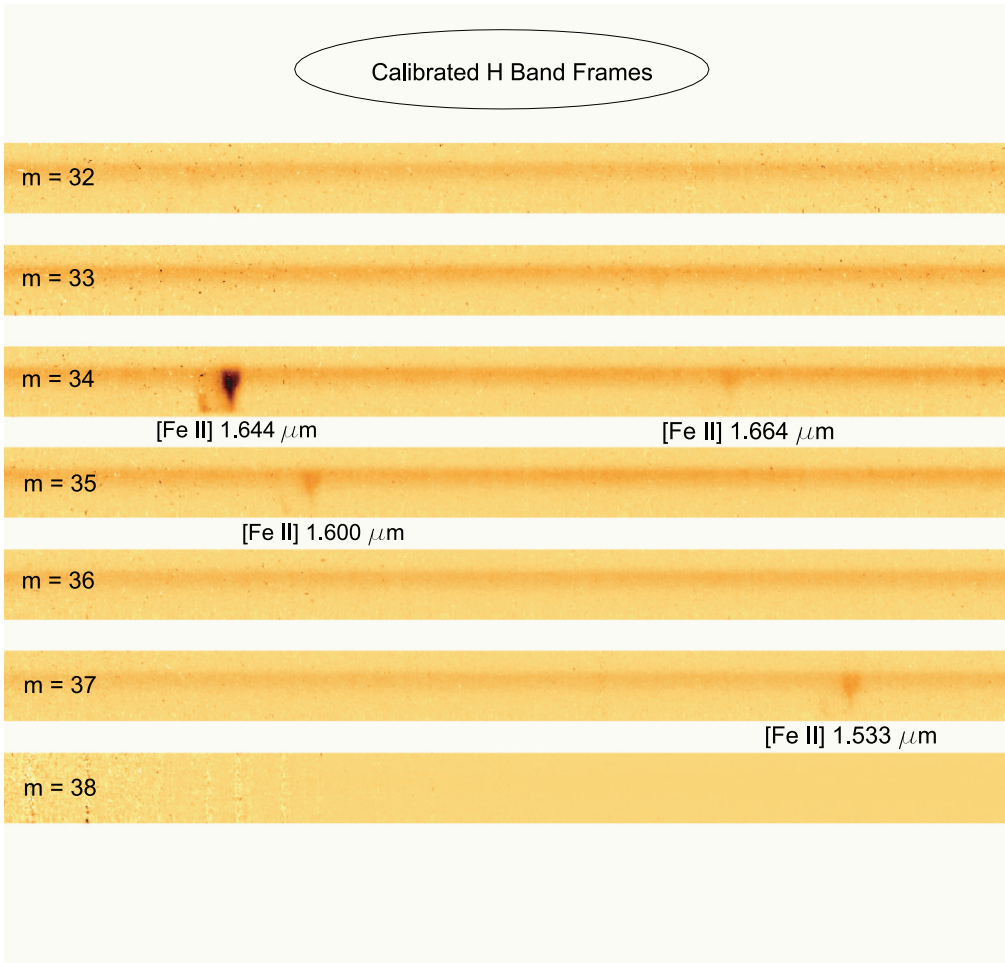
Figure 50: Calibrated apertures. These show the calibrated apertures of the L1551 IRS 5.

5.11 Velocity Correction

An observed spectrum includes the motions of Earth and the Sun, which vary within ± 45 km s^{-1} in V_{LSR} depending on the date of the observation. One can calculate the velocity resulted from these motions by the RVCORRECT task in IRAF. The velocity refferred to the local standard of rest can be obtained by adding the difference of the velocity between the observed velocity and the calculated V_{LSR} to that velocity.

References

Bottema, M. 1981, Ap. Op., 20, 528

Chaffee, F. H., & Schroeder, D. J. 1976, ARAA, 14, 23

Hodapp, K.-W., Hora, J. L., Irwin, E., and Young, T. 1994, PASP, 106, 87

Horne, K. 1986, PASP, 98, 609

Hummer, D. G., & Storey, P. J. 1987, MNRAS, 224, 801

Imanishi, M., Terada, H., Sugiyama, K., Tomita, K., Goto, M., Maihara, T., Kobayashi,
   N., Nagata, T. 1996, PASP, 108, 1129

Kaufer, A. and Pasquini, L. 1998, Proc. SPIE Vol. 3355, p.844

Kitchin, C. R. 1995, Optical Astronomical Spectroscopy, Institute of Physics Publising
   Ltd, London

Load, S. D. 1992, *A New Software Tool for Computing Earth's Atmospheric Transmission
   of Near- and Far-Infrared Radiation*, NASA Technical Memorandum 103957, Ames
   Research Center, California.

Loewen, E. G., Neviere, M., and Maystre, D. 1977, Ap. Op., 16, 2711

Maihara, T., Iwamuro, F., Yamashita, T., Hall, D. N. B., Cowie, L. L., Tokunaga, A. T.,
   & Pickles, A. 1993, PASP, 105, 940

Marsh, T. 1989, PASP, 100, 1032

Massey, P., Valdes, F., & Barnes, J. 1992, *A User's Guide to Reducing Slit Spectra with
   IRAF*, NOAO

Meaburn, J., Blundell, B., Carling, R., Gregory, D. F., Keir, D., and Wynne, C. G. 1984,
   MNRAS, 210, 463

McLean, I. S. 1997, *Electronic Imaging in Astronomy: Detectors and Instrumentation*,
   John Wiley & Sons Ltd in association with Praxis Publishing Ltd, Chichester.

Nussbaumer, H., and Storey, P. J. 1988, A&A, 193, 327

Oliva, E., & Origlia, L., 1992, A&A, 254, 466

Pfeiffer, M. J., Frank, C., Baumüller, D., Fuhrmann, K., and Gehren, T. 1998, A&AS,
   130, 381

Rousselot, P., Lidman, C., Cuby, J. -G., Moreels, G., & Monnet, G. 2000, A&A, 354,
   1134

Schroeder, D. J. 1981, Ap. Op., 20, 530

Schroeder, D. J. 1987, Astronomical Optics. Academic Press, San Diego

Schroeder, D. J., & Hilliard, R. L. 1980, Ap. Op., 19, 2833

Steed, A. J., & Baker, D. J. 1979, Appl. Opt., 18, 3386

Thompson, R. I., Epps, H. W., Winters, G. Womack, W., and Mentzell, E. 1994, PASP, 106, 94

Tokunaga, A. T. 2000, in *Allen's Astrophysical Quantities, 4th edition*, ed. A. N. Cox (AIP PRESS: New York), p150

Tokunaga, A. T., et al. 1998, Proc. SPIE, 3354, 512

Tull, R. G., Macqueen, P. J., Sneden, C., and Lambert, D. 1995, PASP, 107, 251

Valdes, F. 1986, *Reduction of long slit spectra with IRAF*, NOAO

Vogt, S. S. 1987, PASP, 99, 1214

Warren, D. W. 1996, *Baseline Design for the High Resolution Section of the Subaru Infrared Camera and Spectrograph*, The Aerospace Corporation, California

Wheeler, C. C. 1973, *Formulas for Astronomical Grating Spectrographs*, The Perkin-Elmer Corporation, Boller & Chivens Division, South Pasadena

Willmarth, D., & Barnes, J. 1994, *A User's Guide to Reducing Echelle Spectra With IRAF*, NOAO